# ORIGINAL ARTICLE

Giorgio A. Ascoli · Jeffrey L. Krichmar Ruggero Scorcioni · Slawomir J. Nasuto Stephen L. Senft

# **Computer generation and quantitative morphometric analysis of virtual neurons**

Accepted: 9 May 2001

**Abstract** An important goal in computational neuroanatomy is the complete and accurate simulation of neuronal morphology. We are developing computational tools to model three-dimensional dendritic structures based on sets of stochastic rules. This paper reports an extensive, quantitative anatomical characterization of simulated motoneurons and Purkinje cells. We used several local and global algorithms implemented in the L-Neuron and ArborVitae programs to generate sets of virtual neurons. Parameters statistics for all algorithms were measured from experimental data, thus providing a compact and consistent description of these morphological classes. We compared the emergent anatomical features of each group of virtual neurons with those of the experimental database in order to gain insights on the plausibility of the model assumptions, potential improvements to the algorithms, and non-trivial relations among morphological parameters. Algorithms mainly based on local constraints (e.g., branch diameter) were successful in reproducing many morphological properties of both motoneurons and Purkinje cells (e.g. total length, asymmetry, number of bifurcations). The addition of global constraints (e.g., trophic factors) improved the angle-dependent emergent characteristics (average Euclidean distance from the soma to the dendritic terminations, dendritic spread). Virtual neurons systematically displayed greater anatomical variability than real cells, suggesting the need for additional constraints in the models. For several emergent anatomical properties, a specific algorithm reproduced the experimental statistics better than the others did. However, relative performances were often reversed for different anatomical properties and/or morphological classes. Thus, combining the strengths of alternative generative models could lead to comprehensive algorithms for the complete and accurate simulation of dendritic morphology.

**Keywords** 3D models · ArborVitae · Computational neuroanatomy · Dendritic morphology · L-Neuron · Virtual neurons

#### Introduction

The remarkable progress of computer processing power in the last decade has enabled the construction of highly sophisticated models of neuronal function and behavior (Koch and Segev 1998). These models can simulate single-cell electrophysiological features accurately by taking into account many fundamental biophysical and biochemical details, such as membrane properties, ionic channel distributions, and chemical concentrations (Bower and Beeman 1998). Dendritic structure contributes significantly to neuronal information processing (Stuart et al. 1997; Mel et al. 1998) and morphological details may affect the electrophysiological behavior of single neurons (Mainen and Sejnowski 1996). The importance of dendrites for neuronal activity is further evidenced by the influence of dendritic morphology on network connectivity (van Ooyen et al. 2000). Nevertheless, neuronal anatomy has, traditionally, not been modeled in computational neuroscience. Compartmental models of neurophysiology are typically built on a limited set of experimentally traced neurons, or alternatively the neuronal morphology is grossly simplified or disregarded altogether ("ball and stick" models).

The recognition of the crucial role that anatomy plays in supporting and shaping nervous system activity has recently encouraged neuroscientists to develop and characterize computer algorithms for the simulation of neuronal morphology (Senft 1997; van Pelt et al. 1997;

G.A. Ascoli  $(\boxtimes)$  · J.L. Krichmar · R. Scorcioni · S.J. Nasuto S.L. Senft

Krasnow Institute for Advanced Study, George Mason University, MS2A1, 4400 University Drive, Fairfax, VA 22030-4444, USA, e-mail: ascoli@gmu.edu

Tel.: +1-703-9934383, Fax: +1-703-993425

G.A. Ascol

Department of Psychology, George Mason University, Fairfax, Va., USA

G.L. Krichmar, The Neurosciences Institute, 10640 J.J. Hopkins Drive, San Diego, Calif., USA

Winslow et al. 1999; Ascoli and Krichmar 2000). Recent advances in computer graphics have allowed the use of these algorithms to generate and display three-dimensional models of neuronal structures that are anatomically realistic and accurate. Virtual neurons can be used in structure/function relationship studies, as building blocks for biologically plausible neural networks, as tools to search for the most efficient description of neuroanatomical data, or to help investigators develop scientific intuitions and hypotheses (Ascoli 1999; van Pelt et al. this issue).

We are modeling the structure of dendritic trees with a variety of algorithms implemented in two programs, called L-Neuron and ArborVitae (Ascoli et al. 2001). L-Neuron generates dendrites in single cells by local algorithms (Ascoli and Krichmar 2000), in which each simulated dendrite grows depending on intrinsic influences, and independent of other dendritic trees or neurons. The first algorithm implemented in L-Neuron is based on a set of observations and hypotheses originally formulated by Hillman (1979). Dendrites grow by elongation steps of statistically variable length, tapering relative to their diameter. At the end of each step, they either bifurcate or terminate depending on their thickness. If they bifurcate, the daughter diameters are calculated from the parent diameter on the basis of theoretical considerations such as conservation of sectional area or optimization of axial flow (Rall 1959). In a second L-Neuron algorithm, implemented after a model proposed by Burke et al. (1992), dendrites grow by elongation steps of fixed length, tapering at a constant rate. At the end of each step, they can bifurcate, terminate, or elongate again according to a set of continuous, diameter-depending probabilities. If they bifurcate, the daughter diameters are calculated from the parent diameter on the basis of their observed empirical correlations. Both Hillman's and Burke's algorithms, described extensively in the Materials and methods section, follow a local approach because dendritic shape is controlled mainly by the branch diameter, thus disregarding environmental influences (Hillman 1988).

ArborVitae, in contrast, implements global algorithms, in which populations of neurons grow based on global or "environmental" constraints, such as a fixed amount of metabolic resources or the presence of neurotrophic gradients. In global algorithms, the growth of each dendrite is thus influenced by spatial location and by the growth of other dendrites. ArborVitae generates trees by "dealing out" dendritic segments to a population of growing neurons in subsequent phases (Senft 1997; Senft and Ascoli 1999). (In this paper, the term *segment* indicates the minimum cylindrical compartment approximating a piece of dendrite. A branch, in contrast, is a portion of dendrites in between two nodes (stems, bifurcations, or terminal tips). Generally, a branch will be formed by several segments.) In the first phase, segments append to somata (initiating dendrites), and extend to a statistically variable length. In the following phases, the tips of all growing dendrites can bifurcate by receiving a pair of segments in the dealing process. The two attached daughters then receive extending segments until they terminate or bifurcate again. Each growth phase is characterized by a probability of termination and by a "quota" of dendritic length to be assigned. When all the dendrites in a phase quota are dealt out, the next phase is started, until the last phase is over. In this algorithm, which is also described extensively in Materials and methods, the fate of each dendrite depends on that of all other dendrites. Such a global approach reflects a competition among neurons and neurites for growth resources, and is suitable for incorporating *extrinsic* determinants of dendritic shape (Hillman 1988; Senft 1997).

The generation of neuromorphology in L-Neuron and ArborVitae is a stochastic process. When an algorithm uses a parameter (e.g., taper rate), it samples a random number from an appropriate statistical distribution. As a consequence, multiple runs of the same algorithm with a given set of parameters (but with different random seeds), generate different neurons. Such a variability of simulated neurons reflects a natural variability of real cells: even within the same morphological class, no two neurons are identical. Thus, the statistical distributions of the parameters used by the algorithm characterize a neuronal class rather than single individuals. Changing the parameter statistical distributions will change the characteristics of the morphological class (it will describe a different class). Since parameter distributions are extracted, for each morphological class, from experimental data (e.g., from cell tracing reconstructions), stochastic algorithms provide a very compact description of neuroanatomical data (Ascoli et al. 2001).

We call the parameters used by L-Neuron and Arbor-Vitae to generate neuroanatomical structures basic parameters; in contrast, all the morphological parameters not explicitly specified in the algorithms are *emergent* parameters (Ascoli 1999). Taper rate and dendritic stem diameter are examples of basic parameters. Total dendritic surface area and branching order (Uylings et al. 1986) are examples of emergent parameters. Emergent parameters are important to compare virtual cells with the real cells from which the basic parameters were extracted. Such comparison constitutes a fundamental step in the evaluation of morphological algorithms. Analysis of discrepancies between real and virtual neurons can be used to improve the algorithm (i.e., to find better anatomical rules). If the distributions of all emergent parameters of virtual and real neurons are statistically indistinguishable, the algorithm is deemed accurate. In this case, a large population of virtual neurons can be generated to assemble large scale, anatomically accurate neural networks (Senft and Ascoli 1999), or to study the influence of dendritic morphology on neuronal electrophysiology and on axonal navigation (van Ooyen et al. 2000), and can be made available to the neuroscience community through electronic databases (Ascoli et al. 2001).

In recent years, we have used L-Neuron and ArborVitae to generate virtual neurons as diverse as cortical pyramidal cells and thalamic neurons (Senft 1997), hippocampal pyramidal and granule cells (Senft and Ascoli 1999), cerebellar Purkinje cells (Ascoli and Krichmar 2000) and spinal motoneurons (Ascoli et al. 2001). Here, we report the first extensive, quantitative analysis of two classes of virtual neurons, Purkinje cells and motoneurons, generated with various algorithms. Specifically, cells generated with the L-Neuron Hillman and Burke algorithms and with ArborVitae are compared with real neurons. The Purkinje and motoneuron classes were selected for the high quality of the available traced data. In addition, they represent sufficiently different morphologies to provide clues on the generality (or lack thereof) of the conclusions.

# **Materials and methods**

#### Real neuron data

The morphological data of real neurons used in this study consisted of digitized computer files obtained from 3D reconstructions of intracellularly stained cells. The motoneuron files corresponded to six cells from cat spinal cord (Cullheim et al. 1987). The Purkinje cell files corresponded to three neurons from guinea pig cerebellar cortex (Rapp et al. 1994). In both studies, depth (Z) values were corrected for shrinkage and lens medium refraction. The limited number of real neurons does not imply a lack of source data, thanks to the remarkable branching complexity of both motoneurons and Purkinje cells. This dataset contains 1970 motoneuron dendritic branches and 2619 Purkinje cell dendritic branches (from each branch sample, single values of taper rate, branch length, etc. can be measured). All details concerning data availability, formats, and conversions were described elsewhere (Ascoli et al. 2001).

# L-Neuron algorithms

L-Neuron algorithms generate each dendritic tree as an independent process. Each tree stems out of the soma with an initial diameter (basic parameter  $D_{stem}$ ) and orientation (elevation and azimuth, or  $T_{el}$  and  $T_{az}$ , respectively). In the simulation of cells with multiple trees (such as motoneurons), one of the basic parameters is the number of trees per cell (N<sub>tree</sub>; for a summary of all symbols, see the *Glossary* at the end of this section). Once a value n is sampled for this parameter, the algorithm is repeated n times to generate the appropriate number of trees. Every dendritic segment subsequent to the tree stem grows in a direction determined by the growth direction of its parent (the previous segment in the path from the soma), a relative elevation and azimuth determined at bifurcating or extending points, and the influence of tropism, an initial attempt to simulate the effect of neurotrophic gradients (Ascoli and Krichmar 2000). Several types of tropism are implemented in L-Neuron, but only two are used in this study. Somatocentric tropism (TRO<sub>s</sub>) pushes segments away from (or toward, if negative in value) the soma; axial tropisms (TRO<sub>x</sub>, TRO<sub>y</sub>, TRO<sub>z</sub>) push segments towards greater (or smaller) absolute values along a specific Cartesian axis. Tropism only affects growth direction, and no other property, such as length and diameter. The growth direction (with unitary vector length) is modified by adding a tropism direction (with a vector length corresponding to the tropism value, defined between 0 and 1), and the length of the resulting vector is renormalized to 1.

The growth processes in the various L-Neuron algorithms differ in their details. In Burke's algorithm (Fig. 1) dendritic branches grow by a fixed incremental length ( $\Delta L$ ). After growth, the diameter shrinks according to a taper rate (TPR<sub>B</sub>) proportional to the segment length (since  $\Delta L$  is constant, the diameter drop is actually fixed in value throughout growth). Upon elongation, two bifurca-

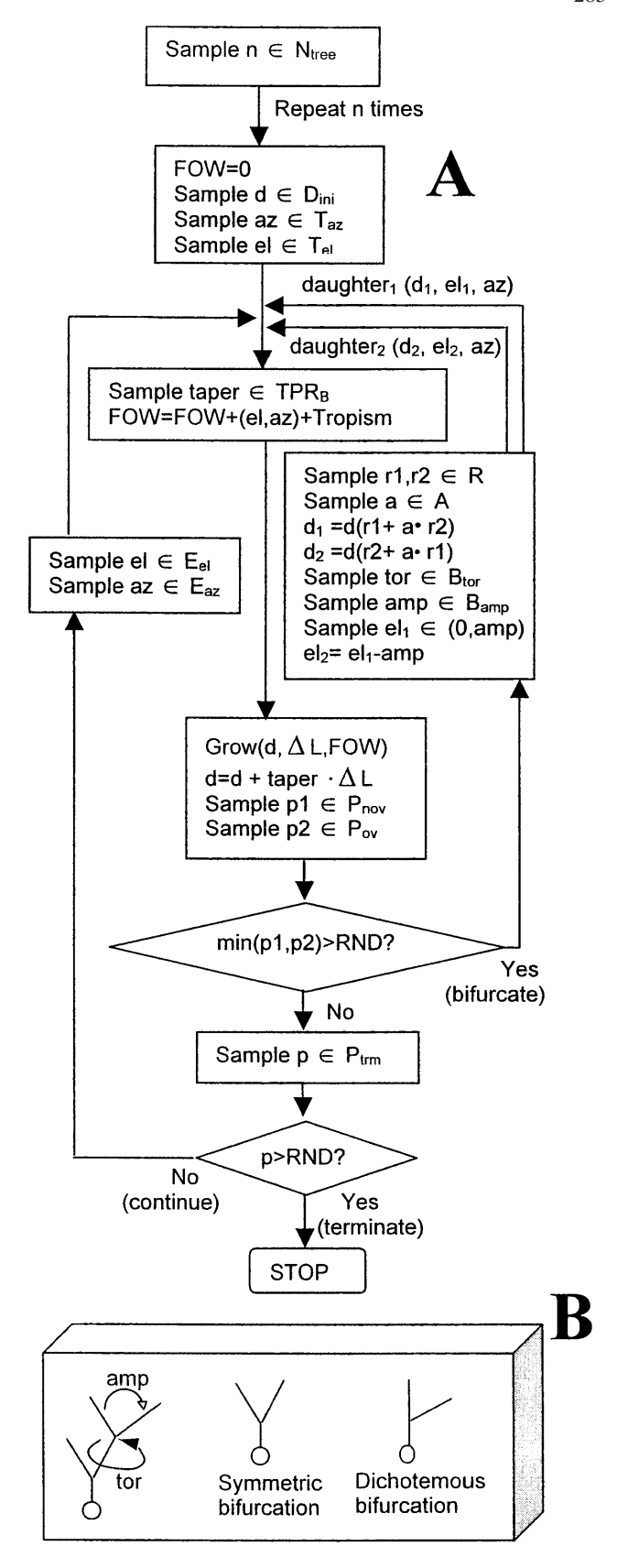


**Fig. 1** A Flow chart of the Burke algorithm in L-Neuron. FOW is the growth orientation vector; see Glossary for all term definitions. **B** Representation of amplitude (amp) and torque (tor) bifurcation angles, and of symmetric and dichotomous bifurcations

tion probabilities are sampled, and the *smaller* of the two is selected. These two probabilities depend exponentially on diameter (see *Glossary* for equations). The first probability is called *overlap* probability ( $P_{ov}$ ) because it is usually selected at small diameters, when branches could also terminate. The second probability is called *non-overlap* probability ( $P_{nov}$ ), because it becomes important at large diameters, when there is no overlapping probability of termination (see Burke et al. 1992, for the rationale). The selected probability ( $P_{ov}$  or  $P_{nov}$ ) is the probability that a dendritic branch bifurcates, creating two daughter branches. The two daughter diameters are calculated by independently sampling two values from the same distribution of a parameter called R by Burke et al. (1992), and linearly combining them with a value sampled from another basic parameter distribution, A (see Fig. 1 for complete equations).

The relative direction coordinates of the two daughters are determined with two parameters (Fig. 1B), a bifurcation torque (B<sub>tor</sub>) and a bifurcation amplitude  $(B_{amp})$ . The azimuth of both daughters is set equal to the torque value. The elevation of one of two daughters is then sampled randomly between zero and the amplitude value, whereas the elevation of the other daughter is set as the complement to the amplitude value, with a negative sign. This implementation of bifurcation angles in L-Neuron rests on two assumptions, namely that the parent and two daughters lie on a plane, and that the "tilt" angle of the bifurcation is randomly distributed between the "symmetric" and "dichotomous" extreme cases (Fig. 1B). Both assumptions are currently being tested. Both daughters of the bifurcation, each with its diameter value and growth direction, repeat the procedure from the unitary growth step described above. If the dendritic branch does not bifurcate, it is assigned a probability to terminate (P<sub>trm</sub>), which also depends exponentially on the local diameter (see Glossary for the equation). If the dendritic branch does not terminate either, the growth direction is updated with elevation and azimuth values sampled from appropriate distributions (E<sub>el</sub> and E<sub>az</sub>, respectively), and the dendritic branch extends with a new segment. The algorithm continues recursively until all branches have terminated.

The L-Neuron implementation of Hillman's algorithm has a similar iterative structure. However, each dendritic branch is generated with a variable length determined by a basic parameter (L<sub>db</sub>). The branch diameter shrinks according to a taper rate (TPR<sub>H</sub>) that is relative to the diameter value itself (i.e., it is a proportional fraction, where 0 corresponds to a cylindrical branch and 1 to a conical branch), but it is independent of the branch length. At this stage, the dendritic branch is broken in a number of segments (Frg) to reflect the natural meandering of real dendritic branches. Each segment is attached to the previous one at an angle appropriate to provide the correct ratio of pathlength over Euclidean distance between the branch starting and ending points ("contraction", or Cnt). The details of this procedure are described elsewhere (Ascoli and Krichmar 2000). After growth, dendritic branches either bifurcate or grow for an additional length (L<sub>trm</sub>) and terminate, depending on whether their ending diameter is larger or smaller than a "threshold" value (Th). The diameters of the two daughters are calculated from the ending diameter of the parent branch using a value of the ratio (DR) between the larger and the smaller of the daughter diameters, and the "power law" (Rall 1959). Rall's law states that the sum of the daughters' diameters, elevated to a power (v) equals the diameter of the parent, elevated to the same power. Empirical observations have actually suggested that Rall's law fits the observed data better if the diameter of the parent, elevated to v, is multiplied by a constant (PK), usually greater than one (e.g. Cullheim et al. 1987). We also implemented this modification of Rall's law in L-Neuron, further imposing the parent diameter as a maximum value for the daughters' diameter. The daughters' growth directions are determined as described for the Burke algorithm. In addition, we also implemented a variation of Hillman's algorithm (Tamori 1993), in which the two daughters' elevation angles are calculated, based on theoretical considerations, from the "effective volume", i.e., a positive quantity whose upper limit is Rall's power  $\nu$  (see Tamori 1993, for the equations, their rationale, assumptions, and proof). In all cases, the two daughters stemming out of the bifurcation, each with given diameter and growth direction, undergo the steps described above as though they were new stems, and the loop is repeated until all branches terminate.

#### ArborVitae algorithm

The population-based approach in ArborVitae is a reflection of the long-term goal of generating and visualizing dense networks of interconnected neurons in an emulation of brain tissue development. The design of ArborVitae approaches this large task in stages by providing methods to: (1) generate, eliminate, migrate, and transform cells; (2) emit and remodel neurites; (3) establish and refine synapses. Here we focus on the aspects of the program that deal with specification of neurites for emulating neuron geometry. Other ArborVitae features have been described elsewhere (Senft 1997: Senft and Ascoli 1999). Dendritic segments in ArborVitae (as in L-Neuron) are represented using tubule primitives, knitted together into trees using a system of parent and child pointers. Each tubule is characterized by its diameter, length, location, and orientation in space. Basic parameters specify elementary segment length ( $\Delta L$ ), initial segment diameter ( $\hat{D}_{stem}$ ), taper rate ( $TPR_B$ ), branch angles (see Glossary and Table 3 for angle symbols). Neuronal structures are created by elementary events (which may be triggered by intrinsic or extrinsic signals) of "appending" a dendritic stem to a cell body, "extending" (with one child) or "bifurcating" (with two children) a pre-existing dendritic segment. We hypothesize that dendritic outgrowth may be described statistically using only a finite number of fundamental "phases" (typically up to five). Each phase is characterized by a set of distinctive statistics constraining the inter-bifurcation pathlengths and the number of branches and terminations (Fig. 2).

The initial growth phase assigns the locations, shapes, and orientations to a set of cell somata. These parameters (x, y, z position in space, elevation and azimuth, diameter and length of the major soma axis) could be derived from morphometry of confocal data (Peterson 1999). Each soma then is dealt a statistically constrained number of initial segments ( $N_{\rm tree}$ ) to begin the arborization process. Segment diameter ( $D_{\rm stem}$ ), length (BrL1) and orientation relative to the soma ( $T_{\rm el}$  and  $T_{\rm az}$ ) are likewise randomly chosen within the statistical distribution characteristic of the initial growth phase. Segments are added onto a *stack* of "actively growing" segments (for efficiency in selecting those growing segments among a rapidly enlarging set of inert ones).

In each subsequent growth phase (generally 2 through 5), items on the active stack are visited in random order, and a topological decision is made to extend, bifurcate or terminate a given segment. Segment identified as extending or bifurcating are linked to the parent; the orientation of the new tip (relative to the parent segment) is resampled from group statistics (Eel and Eaz for extending, Bel and Baz for bifurcating segments). At bifurcations, the orientation of each arm is set independently as a random deviation in elevation and azimuth from the parent vector. Dendrites can be forced to grow in a completely planar way by clamping all bifurcation azimuth values of the two sister segments to zero and 180 degrees, respectively. Extending and bifurcating segments inherit hotspots from their parents. Bifurcating segments also receive an additional hotspot on the stack, which is immediately dealt the second segment to complete the bifurcation. The hotspots of terminating segments are removed from the stack. The frequency and outcome of the topological decision depends both (locally) on variables such as length and diameter and (globally) on the group's current growth phase. The primary local variable is an "inter-bifurcation length" (BrL2 through BrL5), associated with each hotspot. A BrL value is resampled from its phase-specific distribution whenever a neurite appends to a soma or forms a bifurcation; this assigned value decreases by a small amount ( $\Delta L$ ) when each new segment is added. New segments inherit parental diameter, thinned by a taper rate, which corresponds to Burke's parameter TPR<sub>B</sub>. When the inter-bifurcation length is exhausted by the addition of  $\Delta L$  segments, a bifurcate/terminate decision is made de-

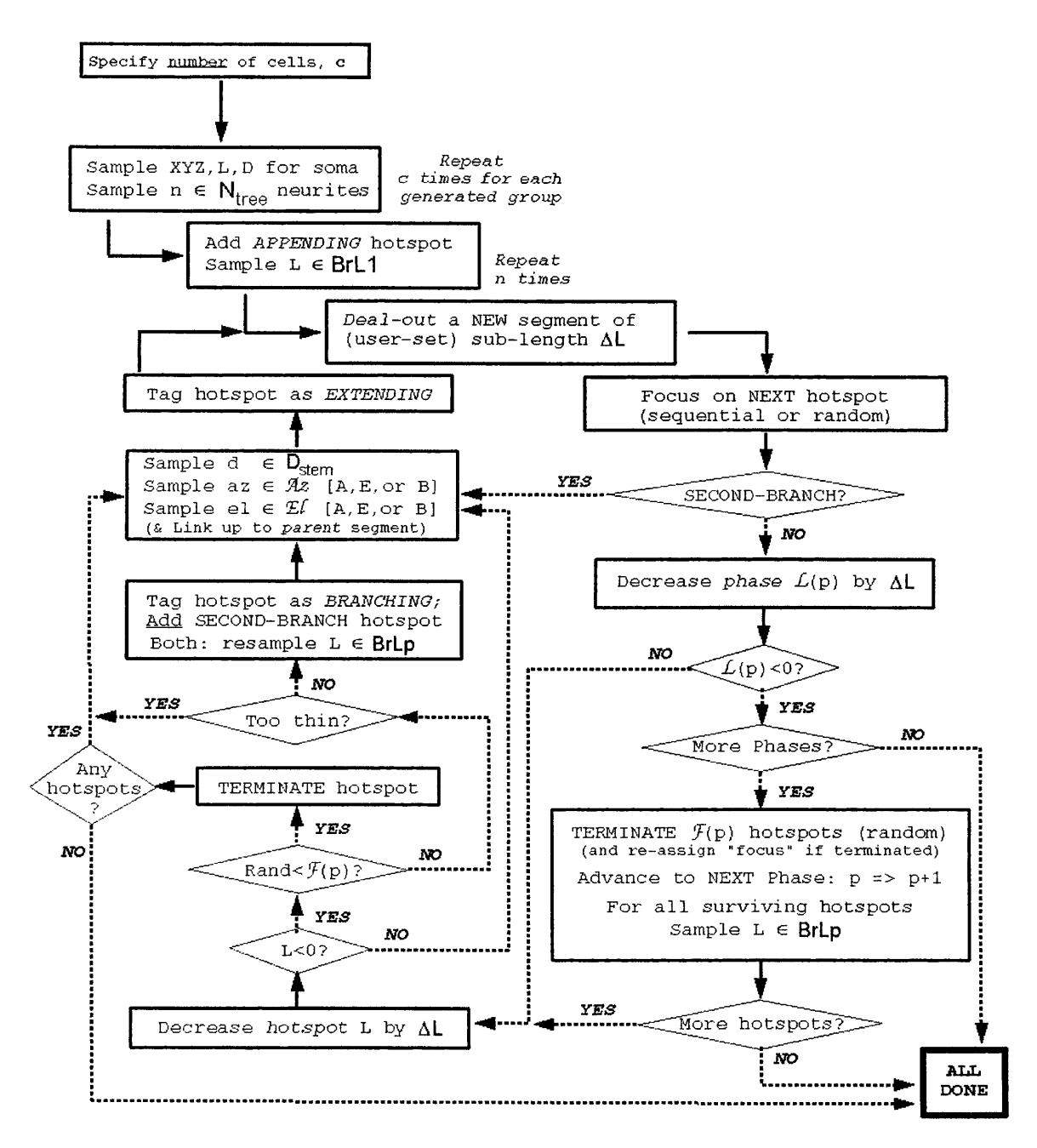


**Fig. 2** ArborVitae algorithm flow chart. The symbol p indicates the phase number. The total length per phase  $\mathcal{L}(p)$  is calculated from the number of branches and their average length (BrLp\*BrBp). The probability of termination  $\mathcal{F}(p)$  is calculated from the numbers of terminations and bifurcations [BrTp/(BrTp+0.5\*BrBp)]. Az [A, E, or B] and El [A, E, or B] indicate azimuth and elevation angles for appending ( $T_{az}$  and  $T_{el}$ ), extending ( $T_{az}$  and  $T_{el}$ ), and bifurcating ( $T_{az}$  and  $T_{el}$ ) segments, respectively

pending on the phase-specific failure probability. Such a probability is calculated from the measured number of bifurcations and terminations [BrT/(BrT+0.5\*BrB), see Glossary for definitions]. In addition, segments whose diameter falls below a threshold value (TD) are prevented from bifurcating, and extend instead.

Each phase is allotted a total length of neurite to deal out to all active tips in the group of cells. Such quantity is calculated from the measured number of branches and their average length

(BrB\*BrL). Every newly added segment decreases this allotment, and the cell group, as a whole, shifts to the next phase when this precalculated quota of neurite has been expended (Fig. 2). Growth ceases when the quota for the last phase is met, or when no more active sites remain on the stack. Multiple groups of neurites (e.g., primary and secondary), each with its own phases, may grow at the same time or sequentially.

#### Basic parameters

The L-Neuron and ArborVitae basic parameters (see Glossary and Fig. 1, 2) can be generally measured from the digitized files of the real (traced) neurons. Such measurements result in distributions of values, which are fitted with a statistical function. Functions used in this study are: (truncated) Gaussian with mean, standard deviation, and optional minimum and maximum values, uniform distribution within a range, or constant value. The truncation of values is important to avoid the stochastic sampling of physically impos-

sible values (e.g., negative diameter). L-Neuron offers the option to define basic parameter distributions as weighted mixtures of two or more statistical functions (see Results for examples). In a few cases, the parameter measurement from the original data is non-trivial. For example, bifurcation amplitude angles  $(B_{\text{amp}})$  are obtained as the arc cosine of the scalar product of the two daughter growth vectors, divided by the product of the two vector lengths. In Hillman's algorithm, these vectors are defined from the bifurcation point to the following bifurcation (or termination) point away from the soma; in Burke's algorithm and in ArborVitae, they are defined from the bifurcation point to the end of the first immediate segment (compartment). Bifurcation torque angles (B<sub>tor</sub>) are calculated from the scalar product of the two vectors obtained as the cross products of the daughter growth vectors of the given bifurcation and the daughter growth vectors of the previous bifurcation towards the soma (Fig. 1B). The torque angle of the first bifurcation, as well as the elevation and azimuth angles of dendritic trees (T<sub>el</sub> and T<sub>el</sub>), are arbitrarily defined with respect to the orientation of the Cartesian z axis (in L-Neuron, somata are spherical and centered in the origin of the Cartesian coordinates). The extraction of Burke's parameters is described at length in the literature (Burke et al. 1992), and need not be discussed further. The growth step length in Burke's algorithm,  $\Delta L$ , is not measured, but rather set to achieve a balance between computational efficiency and length resolution. Within a restricted range of this parameter around the value used to measure bifurcation and termination probabilities, the exact value of  $\Delta L$  has no significant effect on the statistics of the simulated morphology. Other technical details regarding the extraction of Hillman's parameters are reported elsewhere (Ascoli 2001).

Basic parameters describing global effects may be difficult to measure directly from digitized neurons, but can be found by minimizing the error of one or more emergent parameters (e.g., van Pelt et al. 1997). For example, tropism values are added to the L-Neuron models to reduce the discrepancies observed between real and virtual neurons, and a parameter search can be run to optimize their values. Similarly, the division into growth phases in ArborVitae are hard to estimate from real neuron data. Assuming that dendritic branches closer to the soma have developed earlier, on average, in the growth process of real neurons, ArborVitae phases can be approximately derived from discontinuities in the plot of the number of bifurcations or terminations versus distance from the soma (see Results for an example). The segments contained within each phase are then analyzed to extract the statistics used by the growth algorithm. Growth phases could also be estimated by simulating the progressive erosion of all traced dendrites from the tips inward. Assuming an approximately uniform rate of growth for the group of cells as a whole, one could then build a map of the time of addition for each region of neurite, and partition this map into phases. We should finally note that some of the basic parameters (e.g., initial stem diameter  $\boldsymbol{D}_{\text{stem}}\!)$  are common to several algorithms, whereas others (e.g., Burke's termination probability P<sub>trm</sub>) are specific for a certain algorithm. These latter parameters can be considered emergent for the algorithms in which they are not employed.

#### Emergent parameters

Emergent parameters are all morphological parameters that are *not* explicitly specified in a dendritic growth algorithm, but "emerge" from the growth of virtual neurons. Some of these parameters may be interdependent; for example, the total number of terminations and the total number of bifurcations in a neuron are both emergent parameters, but their difference equals the number of dendritic trees in that neuron, which is a basic parameter. Classical neuroanatomical analyses of dendritic morphology adopt sets of orthogonal (or non-interdependent) parameters (Uylings et al. 1986). We typically use a large number of emergent parameters to compare virtual and real neurons. Here, we distinguish two types of emergent parameters, namely *scalar* parameters and *distribution* parameters. Scalar parameters encapsulate a feature of dendritic

morphology in a single number. An example of scalar emergent parameter is the total number of bifurcations in a neuron. Distribution parameters characterize a structural aspect of neurons by the dependency of a morphological quantity on another morphological variable. An example of distribution emergent parameter is the peak position of the plot of number of bifurcations versus distance from the soma (Sholl 1953).

Eleven scalar emergent parameters were used in this study: total dendritic length, total surface area, topological asymmetry, total number of bifurcations, maximum branching order, average path from soma to tips, average distance from soma to tips, maximum distance from soma to tips, significant height, significant width, and significant depth. The topological asymmetry (van Pelt et al. 1992) is the average of the partition values over all the bifurcations of the neuron. The partition is defined as the difference of the numbers of terminations descending from each of the two daughters of a bifurcation, divided by the total number of terminations descending from that bifurcation minus two. The partition value is zero for totally symmetric bifurcations (with an identical number of terminations descending from each daughter) and one for totally asymmetric bifurcations (with one directly terminating daughter and the rest of the tree descending from the other daughter). The branching order at any point in the dendritic tree is the number of bifurcations encountered in the path to the soma, plus one. It is important to notice that this is a purely topological definition, and it does not take into account any "weight" for the daughter diameters. Thus, the branching order of a thick trunk with many outgrowing thin branches is affected by each branch, even if its diameter remains almost unchanged by the bifurcations (e.g., Uylings et al. 1986). The path measures a length along the dendrite, whereas distance here means a Euclidean distance between two points. The significant height (and analogously the width and depth) of a neuron is the minimum height of a large and deep box that would contain 95% of the dendritic segments, leaving out only 2.5% of the trees on each side.

The total dendritic length, total surface area, topological asymmetry, total number of bifurcations, maximum branching order, and average path from soma to tips only depend on dendritic topology and local size (segment diameter and length), but not at all on angles and space packing (i.e., they are "isometric" parameters). In contrast, the average distance from soma to tips, maximum distance from soma to tips, significant height, significant width, and significant depth are influenced by angles as well as by topology and lengths. These eleven parameters together provide a compact and informative "snapshot" of dendritic morphology, and can be used for a preliminary assessment of the matching between groups of real and virtual neurons.

Three types of distribution emergent parameters were analyzed in this study: the dependency of morphological quantities on branching order, path distance from the soma, and Euclidean distance from the soma. The morphological quantities examined included the average number of bifurcating or terminating segments (at a given order, or in a bin of distance), the average dendritic branch diameter, the total dendritic length or area, and the average bifurcation partition. Occasionally, the cross-distributions were also examined, e.g., the distribution of the average distance from the soma of the segments at a given order, versus the order, or vice versa. The examination of distribution parameter plots provides an extremely detailed characterization of morphological features. Depending on the distribution shape, distribution parameters can also be described quantitatively in different ways. For example, bellshaped distributions are typically characterized with the position of the distribution peak and with the peak width at half-height, while linear distributions can be characterized with slope and intercept.

#### Implementation and availability

The L-Neuron program is coded in C++ (Ascoli and Krichmar 2000) and it can be compiled under both Windows/DOS and Unix systems (Irix and Linux). The Window/DOS version is bun-

dled with Laurens Lapré's pseudo-3D display software L-Viewer and is to be freely distributed through the L-Neuron web site (www.krasnow.gmu.edu/L-Neuron, case sensitive). All the L-Neuron simulations reported in this study were run under DOS on a 433 MHz Pentium III computer with 128 MB of RAM. An average size neuron was generated in approximately 2 s of clock time (roughly 2500 segments per s). The ArborVitae program is coded in C/GL (Senft, 1997), and it runs under the Irix operating system. The simulations reported here were run on a 75 MHz R8000 Silicon Graphics Indigo 2 with 320 MB of RAM. A typical simulation producing a group of ten neurons took approximately 30 s (roughly 1500 segments per s). The routines to convert motoneuron files from the original digitized format to SWC, and the Purkinje cell files from Eutectic format to SWC, were written in the AWK programming language and ran under Unix, as previously described (Ascoli et al. 2001). The programs to extract Hillman, Burke, and ArborVitae basic parameters from the digitized data in SWC format were also written in AWK under Unix. The software to extract emergent parameters from real and virtual neurons in SWC format was written in C++ and ran under DOS. All conversion routines and programs to extract basic and emergent morphological parameters from digitized data are have been subsequently ported in C++ in a single object of the L-Neuron code. This software tool is freely distributed through the L-Neuron web site as a stand-alone utility called L-Measure (Scorcioni et al. 2001). All the (real and virtual) neurons used in this study are stored in SWC format in an electronic database (Ascoli et al. 2001), and publicly available at www.krasnow.gmu.edu/L-Neuron (case sensitive).

Glossary	
A	Parameter for the linear combination of values to
$\begin{array}{l} B_{amp} \\ B_{az}(B_{el}) \end{array}$	obtain the daughters' diameters [Burke] Amplitude angle in a bifurcation [Burke, Hillman] Azimuth (elevation) angle for daughter branches
$\begin{array}{c} B_{tor} \\ BrL1 \end{array}$	relative to the parent [ArborVitae] Torque angle in a bifurcation [Burke, Hillman] Dendritic stem length from the soma to the first bifurcation [ArborVitae]
BrLp	furcation [ArborVitae] Pathlength between two consecutive bifurcations (obetween a bifurcation and a termination) in the pt
BrTp(BrBp)	growth phase (p=25) [ArborVitae] Number of terminations (daughter branches) in th pth growth phase [ArborVitae]
Cnt	"Contraction" ratio between pathlength and Euclide an distance between two bifurcation points [Hill
$\mathbf{D}_{\mathrm{stem}}$	man] Initial diameter of the dendritic tree [ArborVitae Burke, Hillman]
$\begin{array}{l} DR \\ E_{az}(E_{el}) \end{array}$	Daughter diameter ratio (larger/smaller) [Hillman] Azimuth (elevation)angle in extending dendriti
Frg	segments [ArborVitae, Burke] Number of fragments in which each dendritic segment is divided [Hillman]
$L_{db}$ $L_{trm}$	Inter-bifurcation pathlength [Hillman] Additional length at terminating branches [Hillman]
$N_{\text{tree}}$ $P_{\text{nov}}$	Number of dendritic trees per soma [ArborVitae Burke, Hillman] "Non-overlap" bifurcation probability, correspond
P <sub>ov</sub>	ing to $k1_{nov}$ *exp( $k2_{nov}$ ) [Burke] "Overlap" bifurcation probability, corresponding to
$P_{trm}$	k1 <sub>ov</sub> *exp(k2 <sub>ov</sub> ) [Burke] Termination probability, corresponding to k1 <sub>trm</sub> *exp
PK R	(k2 <sub>trm</sub> ) [Burke] Power constant modifying Rall's law [Hillman] Distribution of values to be linearly combined to ob
$T_{az}(T_{el})$	tain the daughters' diameters [Burke] Azimuth (elevation) angle of the dendritic tree ster
Th	[ArborVitae, Burke, Hillman] Threshold diameter between terminating and bifur cating branches [Hillman]

TD	Minimum	diameter	to	allow	bifurcating	events
	[ArborVita	el .				

TPR<sub>B</sub>(TPR<sub>H</sub>) Taper rate [ArborVitae, Burke (Hillman)]

TRO<sub>s</sub> Tropism towards (or away from) the soma [Hillman] Tropism towards greater (or smaller) absolute val-TRO<sub>v</sub>

ues in the x coordinate [Hillman]

Branch incremental growth length [ArborVitae,

Power coefficient in Rall's law [Hillman]

# **Results**

# Analysis of basic parameters

All L-Neuron and ArborVitae basic parameters were measured from digital files of traced neurons. Raw data for each parameter were extracted in the form of simple arrays and characterized with histograms representing frequency distributions. The distribution type (e.g., Gaussian, uniform, exponential, etc.) was then visually determined, and the histograms were fitted with the appropriate functions. The best fitting parameters of these functions constituted the values of the corresponding statistical distributions of basic parameters. Four examples of this procedure are reported here (Fig. 3).

The distribution of the length of dendritic branches between bifurcations (L<sub>db</sub> in the Hillman algorithm of L-Neuron) from the six original motoneurons is shown in Fig. 3A. The range of experimental values (between 10 and 600 µm) is distributed unevenly in a skewed bellshape with a long right-tail. Such a distribution was fitted with a Gaussian function truncated at a minimum threshold. The best fitting computation yielded values of 50 µm for the mean, 150 µm for the standard deviation, and 10 µm for the minimum threshold. While the value for the minimum reflects the experimental observation, the mean value for the Gaussian distribution does not correspond to the plain average of the experimental values, because of the skewness of the data. To control for accuracy, an amount of random numbers equal to the number of experimental observations was generated with a truncated Gaussian function according to the fitted values, and overlaid on the original data (Fig. 3A). The range, skewness, and peak position of real and generated data correspond satisfactorily.

The second example of basic parameter extraction involves the dependency of the bifurcating and terminating probabilities (per unit of length) on branch diameter in the L-Neuron Burke algorithm. These probabilities are calculated by grouping all branches in bins depending on their diameters, and then dividing the number of bifurcations and terminations in each bin by the total dendritic length in that bin (Burke et al. 1992). The extraction of these values from motoneurons yielded results in excellent agreement with those reported by Burke et al. (1992). In particular, the termination probability could be fitted with a diameter-dependent exponential decay, while the bifurcating probability was fitted with two exponential functions with different steepness: a rapidly in-

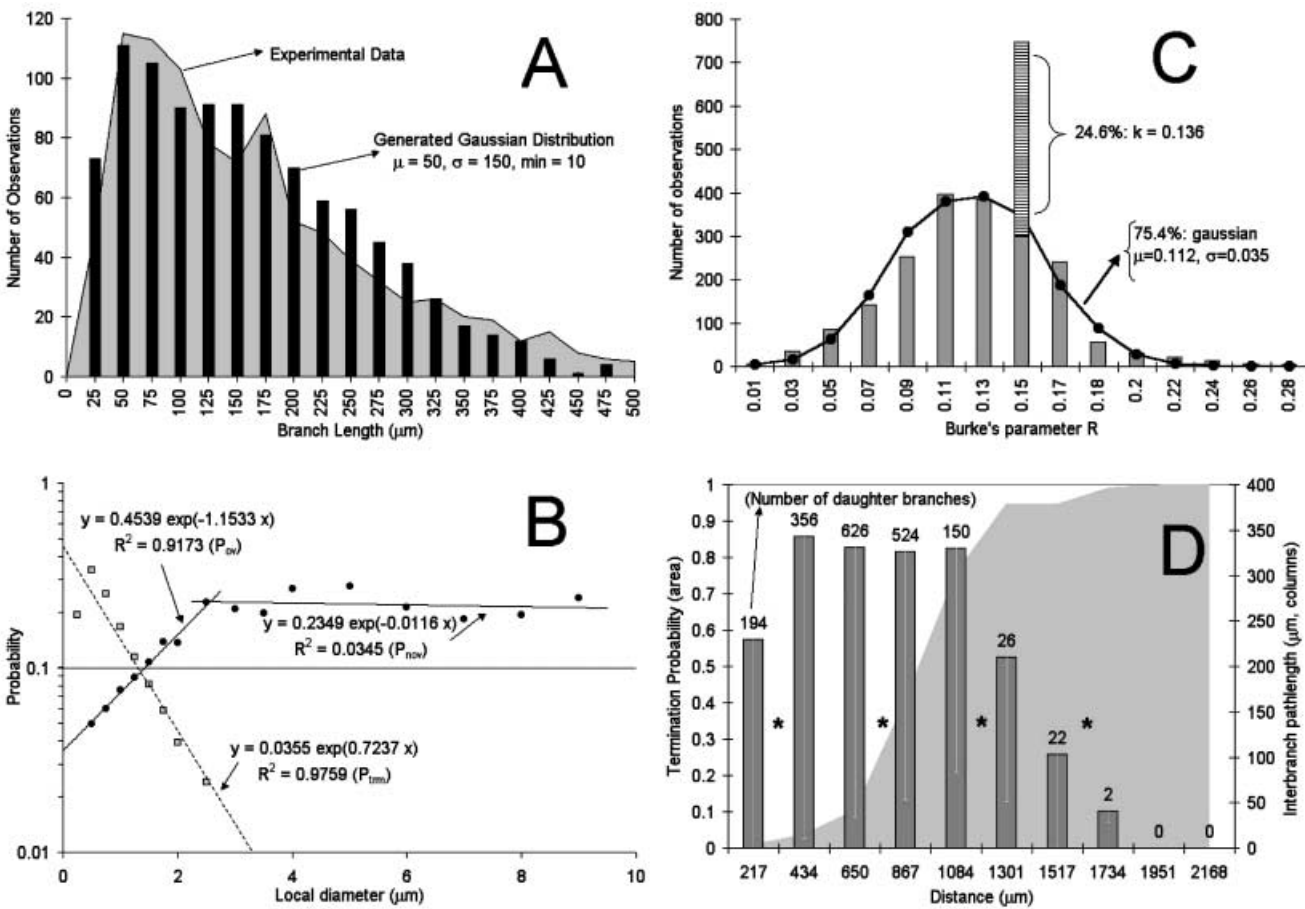


Fig. 3A–D Examples of data analysis for the extraction of basic parameters from experimental data. A Fitting of motoneuron branch length with a truncated Gaussian distribution (Hillman algorithm): experimental (gray area) and generated data (dark columns). B Characterization of diameter-dependent terminating (gray squares) and bifurcating (black dots) probabilities as exponential functions in Purkinje cells (Burke algorithm). C Description of the observed R distribution in Purkinje cells (columns) as a mix of a Gaussian function (line; the dots represent stochastically generated data) and a constant value (striped). D ArborVitae motoneuron parameters at varying path distances from the soma. Variations of the fraction of terminating branches (area), number of daughter branches (labels), and mean (column) and standard deviation (inner bars) of branch length are used to select the growth phase divisions (asterisks)

creasing function at diameter values overlapping with the terminating range, and a slower exponential function at larger diameters (data not shown). The analogous data extraction from Purkinje cells (Fig. 3B) resulted in qualitatively similar results to those obtained with motoneurons. Specifically, terminating and bifurcating probabilities could be fitted with three exponential functions. In the "overlapping" region, the slope of the terminating probability was negative, while that of the bifurcating probability was positive (note logarithmic scale in Fig. 3B, and compare to Fig. 2B in Burke et al. 1992). In the "non-overlapping region", the bifurcating probability reached a nearly constant value. As an additional indication of the applicability of Burke's analysis to Purkinje cells, we also report the extraction of Burke basic param-

eter "R", used in the generation of daughter diameters at bifurcation points. In motoneurons, this distribution was fitted by a Gaussian function (data not shown, but see Fig. 6B in Burke et al, 1992), with values identical to those in the literature (Burke et al. 1992). In Purkinje cells, the values of R yielded a bell shaped function deformed by a narrow peak on the right tail (Fig. 3C). Once the values corresponding to this peak (24.6% of all the data points) were set aside, the remaining data could be described with a regular Gaussian distribution. Thus, this basic parameter for Purkinje cells consists of a mixture of two distributions.

A last example of basic parameter extraction is the phase division in ArborVitae (Fig. 3D). The fraction of terminating branches, number of daughter branches, and mean and standard deviation of branch length are measured as a function of path distance from the soma. The main points of discontinuity in these parameters are taken as the divisions in growth phases. Within each phase, values for each parameter are then averaged and used uniformly. For motoneurons, the first phase separated out in all parameters (see asterisks in Fig. 3D). Second and third phases had similar number of bifurcations and branch length, but different termination probability. The fourth and fifth phases were divided on the basis of branch number and length.

Following procedures similar to those exemplified above, all basic parameters were extracted for the three algorithms (L-Neuron's Hillman and Burke, and Arbor-

**Table 1** L-Neuron basic parameters (see Glossary and Fig. 1A for parameter definitions). Distribution types are uniform (U), Gaussian (G), and constant (K). For truncated Gaussian distributions, generated points are sampled as regular Gaussian with mean  $(\mu)$ 

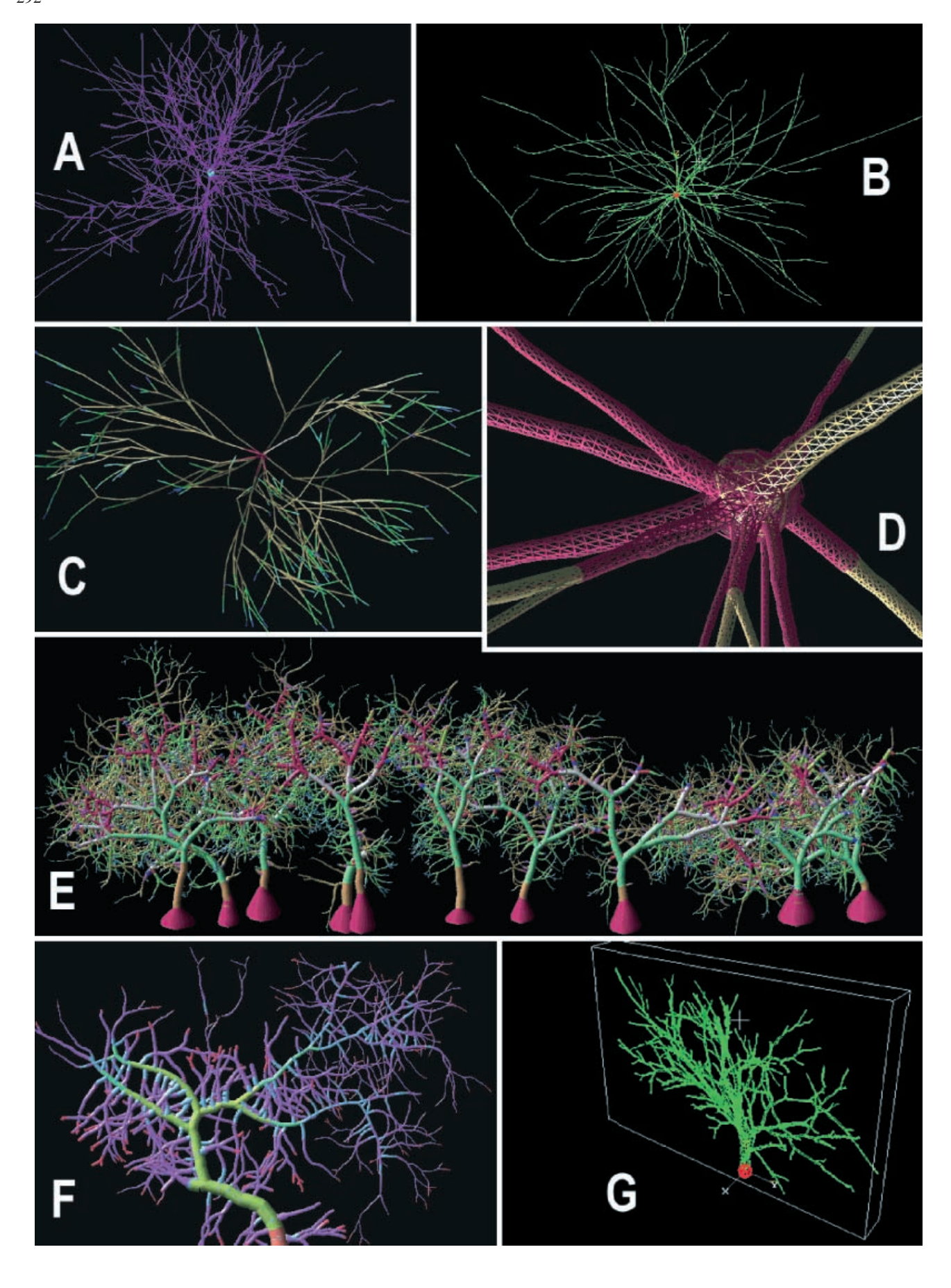
and standard deviation ( $\sigma$ ) values, and then discarded if not within the range (min-max). Values marked with an \* are taken from the literature (Cullheim et al. 1987)

Cell Type	Motoneu	rons				Purkinje				
Param.	Dist	μ	σ	Min	Max	Dist	μ	σ	Min	Max
N <sub>tree</sub>	U			8	16	K	1			
$D_{\text{stem}}^{\text{tree}} (\mu \text{m})$	58% U			3	12	75% G	6.167	1.069	4.8	7.6
stem 4	42% U			5	10	25% U			5.5	7.4
T <sub>el</sub> (deg)	U			0	180	K	0			
T <sub>az</sub> (deg)	U			-180	180	K	0			
$L_{db}^{az}$ (µm)	G	50	150	10	1200	G	9.5	5.7	0.5	44
TPR <sub>H</sub>	62% G	0.3	0.3	-1.3	1	79% K	0			
11	38% K	0				14% U			0.05	0.4
						7% G	-0.17	0.19	-1.8	0
$TPR_{B} (\times 10^{3})$	K*	-125				49% K	0			
В 、 /						45% G	-10	22		
						6% U			50	20
Frg	G	2	1	1		G	0	1.56	0.39	
Cnt	52% K	1				53% K	1			
	40% G	1	0.1	0.1	1	47% G	1.1	0.1	0.3	0.99
	8% U			0.5	0.8					
Th (µm)	96% G	1.125	0.8	0.45	9.27	90% G	1.02	0.269	0.3	2.7
4. /	4% K	0.875				10% U			1.5	2.2
L, (um)	U			50	500	K	0.1			
$L_{trm}$ ( $\mu m$ )	Ğ	1.3	0.8	1	10	G	1.18	0.68	1	
PK	K*	1.13*		_		74% G	1.14	0.5	0.25	5
		1.13				26% K	2	0.0	0.20	-
B <sub>tor</sub> (deg)	U			0	180	G	0.0	13.5		
$B_{amp}$ (deg)	Ğ	45	20	1	172	Ğ	71	40	1	179

**Table 2** ArborVitae basic parameters (^planarity imposed) (see Glossary and Fig. 2 for parameter definitions). Azimuth angles ( $T_{az}$ ,  $E_{az}$ ,  $B_{az}$ ) were left unconstrained for motoneurons, and set to zero for Purkinje cells (with the additional imposition of planar-

ity). For Purkinje cells, values in parentheses are for secondary dendrites. Where parentheses are not specified, the same values apply for both primary and secondary dendrites

Cell Type Motoneurons						Purkinje primary (secondary)				
Param.	Dis	μ	σ	min	Max	Dis	μ	σ	min	Max
N <sub>tree</sub>	G	11.67	0.2	5	15	K	1			
BrL1 (µm)	G	161.1	118.8	39	512	G	7.3(1.3)	29.6	16.9	74.9
BrL2 (µm)	G	317.8	302	9.8	10664	G	14.4(4.4)	10.3	3.8	29
BrB2	K	196				K	6.66(3.66)			
BrT2	K	7.5				K	0.1(0.5)			
BrL3 (µm)	G	326.6	273	4	1241	G	9.69(1.69)	6.67(0.67)	0.87	40.7
BrB3	K	87.33				K	7.33(3.33)			
BrT3	K	30				K	2.66(0.66)			
BrL4 (µm)	G	330.3	246.2	11	1292	G	10.25	7.76	5	63.21
BrB4	K	25				K	8.6666			
BrT4	K	39.33				K	0.3333			
BrL5 (µm)	G	156.5	130.9	15	727.4	G	11.87	9.1	1.11	54
BrB5	K	8.333				K	5.3333			
BrT5	K	93.16				K	3			
$TPR_A$	K	0.45				K	0.025(0.03)			
$D_{\text{stem}}^{R}(\mu m)$	U			2	15	U	` ,		4(1)	5.75(3)
TD (µm)	K	1.75				K	0.75(0.35)		. ,	. ,
ΔL (μm)	K	75				G	2(0.65)	0.5(0)	10	
T <sub>el</sub> (deg)	U	-360	360			U^	, ,	. ,	0(75)	0(105)
B <sub>el</sub> (deg)	G	22.5	10	0.5	86	$G^{\wedge}$	34.5(28.5)	9(5)	1	179
E <sub>el</sub> (deg)	G	0	5			$G^{\wedge}$	0	6(10)		



Vitae) and the two cell classes (motoneurons and Purkinje cells). The complete set of these data, as used in all subsequent simulations, is summarized in Tables 1 and 2. Table 1 reports the statistical functions of L-Neuron basic parameters for motoneurons and Purkinje cells. The motoneuron values of the additional parameters specific for Burke's algorithm coincide with the literature (Burke et al, 1992). Corresponding values for Purkinje cells can be derived from Fig. 3B, C. Table 2 contains the basic ArborVitae parameters. Notice that Purkinje cells were modeled with two levels of dendrites, primary and secondary, to account for observed discontinuities in diameter and in bifurcation angles that could not be described with the simple phase sequence. Primary dendrites appended to the soma, while secondary dendrites appended to the primary ones.

#### Generation of virtual neurons

Since the original datasets consisted of a limited number of neurons (six motoneurons and three Purkinje cells), we generated larger sets of virtual neurons to allow a statistical analysis of their scalar emergent parameters. For each algorithm (Hillman, Burke, ArborVitae), ten or more datasets of virtual neurons were produced. Each simulated motoneuron set contained six exemplars, while each simulated Purkinje cell set contained three exemplars. The scalar emergent parameters were measured from each real and virtual neuron. Every group of six or three was statistically characterized with mean, minimum, and maximum values for each of the scalar parameters. Virtual data were then analyzed in terms of average and standard deviation of each value, and compared to the corresponding values of the experimental group (see e.g., Table 4). In general, the three-dimensional display of simulated neurons, as well as a more advanced visual inspection (including rotation, zooming, color rendering of individual arbors, etc.) demonstrated that generated structure attained a remarkable level of anatomical realism. In several cases, it was difficult to distinguish between computer rendering of real and virtual neurons. Examples of the simulated structures are shown in Fig. 4. Panels A-C represent motoneurons generated with the Hillman, Burke, and ArborVitae algorithms, respectively. Because of the large size of dendritic arbors in motoneurons, the details of tree stems and somata are not visible in the entire neurons. **D** displays a close-up of the soma with 11 stemming dendrites from

◆ Fig. 4A-G Examples of virtual neurons. A Motoneuron generated with L-Neuron Hillman/PK algorithm. B Motoneuron generated with L-Neuron Burke algorithm. C Motoneuron generated with ArborVitae (growth phases are color-coded). D Enlargement of the dendritic stems from C. E Ten Purkinje cells generated by ArborVitae (colors as in C). F Enlargement of a dendritic tree from E. G An L-Neuron Purkinje cell generated with the Tamori/Hillman algorithm. The quasi-planarity is imposed by the additional influence of tropism

C. E shows a population of ten Purkinje cells generated with ArborVitae. Despite their overall resemblance, the ten exemplars, generated stochastically using a single set of statistical distributions of basic parameters, are individually different. F is an enlargement of one of the dendrites from E. Different colors mark dendrites grown in different phases of the algorithm. G displays a Purkinje cell generated by the Tamori variation of the Hillman algorithm, with the additional influence of tropism. The neuron is entirely enclosed in a virtual "box" in order to highlight the relative width, height and depth of the dendrites.

# Analysis of motoneuron emergent parameters

The quantitative analysis of scalar emergent parameters for motoneurons is reported in Table 3. The "plain" version of Hillman's algorithm (without the PK correction to Rall's power law) generated neurons that were significantly smaller than the real cells. The means of total length and of number of bifurcation for Hillman motoneurons were less than 70% of those of real motoneurons (standard deviations only amounted to <10% of the means). The maximum value of surface area for Hillman motoneurons was lower than the minimum corresponding value in real cells. Nevertheless, the Hillman algorithm captured some of the emergent properties of real motoneurons, such as the mean, minimum and maximum values of asymmetry. The PK correction of Rall's law greatly improved the Hillman algorithm. The average of most parameter mean values of the corrected Hillman algorithm fell within 1 or 1.5 standard deviations from the experimental data. In particular, the dendritic length, asymmetry, branching order, average path and distance from soma to tips, and the height/depth of real motoneuron were all quantitatively reproduced in virtual neurons. However, the mean surface area and width indicated that Hillman's neurons were still smaller than the real ones. As a general trend, the range (max-min) of many emergent parameters was wider for virtual neurons than for real cells (Table 3).

Burke's algorithm yielded results similar to the corrected Hillman algorithm. Most parameter mean values had averages and deviations compatible with the original data. With respect to Hillman/PK motoneurons, Burke's dendrites were shorter and had fewer bifurcations, but had a larger surface. However, Burke's algorithm failed to reproduce the experimental values related to overall tree size (e.g., maximum distance to tips and tree depth). As with Hillman's algorithm, Burke motoneurons had wider ranges of values (in most parameters) than the real cells. ArborVitae motoneurons reproduced several emergent characteristics of traced neurons (e.g. minimum length and area values, minimum, maximum and mean asymmetry), but were larger than the real cells, as assessed by the mean of all size-related parameters. Although this trend is opposite to that shown by the L-Neuron algorithms, the variability of ArborVitae neurons,

**Table 3** Scalar emergent parameters for motoneurons. Six real motoneurons and 10 groups of six motoneurons for each algorithms were analyzed. Mean, minimum and maximum values refer

to measurements within a group of six cells. The average and standard deviation ( $\mu\pm\sigma$ ) for virtual neurons refer to measurements of each value (mean, min, max) within a set of 10 groups

Parameter	Value	Exp. ( <i>n</i> =1×6)	Hillman (n=10×6) μ±σ	Hillman/Poliko (n=10×6) μ±σ	Burke ( <i>n</i> =10×6) μ±σ	ArborVitae (n=10×6) μ±σ
Total length (µm)	Mean	102,799	67,255±6002	94,609±10213	87,876±7230	116,972±7971
	Minimum	78,849	41,510±9153	58,311±9025.4	66,660±9062	77,878±14,455
	Maximum	117,030	91,753±12,102	136,278±21,529	117,902±15,234	162,211±22,373
Total area (μm²)	Mean	562,363	287,802±28,245	401,511±46,572	464,713±38,049	721,219±50,655
	Minimum	499,675	174,102±39,512	248,227±40,614	354,959±41,453	488,928±76,317
	Maximum	676,398	401,798±56,457	573,031±94,975	628,177±84,496	985086±126563
Asymmetry	Mean	0.462	0.46±0.02	0.48±0.01	0.42±0.01	0.46±0.01
	Minimum	0.420	0.42±0.02	0.45±0.02	0.38±0.01	0.43±0.02
	Maximum	0.510	0.51±0.02	0.52±0.01	0.45±0.02	0.49±0.02
No. of Bifurcations	Mean	158.3	111.1±11.2	159.7±18.28	122.4±9.91	196.6±13.64
	Minimum	122.0	69.3±16.8	96.4±16.43	92.0±11.05	121.5±27.94
	Maximum	181.0	152.8±23.3	233.7±40.50	165.2±19.37	280±39.94
Maximum order	Mean	10.3	9.3±0.3	11.8±0.74	9.2±0.31	12.7±0.50
	Minimum	10.0	8.0±0.7	9.8±0.6	7.6±0.49	10.7±0.92
	Maximum	12.0	11.1±0.4	13.6±1.2	11.0±1.01	15.2±1.41
Average path to tips (µm)	Mean	1137.1	1035.2±32.13	1153.4±31.43	1199.2±27.73	1753.82±48.58
	Minimum	1090.4	903.1±59.26	1058.3±38.04	1103.8±33.41	1635.77±101.21
	Max	1178.8	1153.8±67.99	1289.8±99.64	1346.1±92.83	1877.791±72.24
Average distance to tips (µm)	Mean	932.7	874.36±21.8	953.3±23.7	1055.4±22.3	1560.61±45.17
	Minimum	874.7	771.26±45.3	880.3±35.2	971.2±27.1	1451.69±89.37
	Maximum	1007.8	958.42±38.1	1052.0±76.4	1169.9±69.4	1662.22±60.45
Maximum distance to tips (μm)	Mean	1615.6	1662.39±79.44	1858.0±81.26	2348.1±105.79	2507.81±89.57
	Minimum	1531.5	1323.04±133.09	1621.4±130.19	2081.4±115.64	2283.93±90.23
	Maximum	1713.4	2018.98±207.73	2161.1±162.10	2683.9±199.33	2812.11±134.3
Height (95%)	Mean	1600	1397.25±111.75	1565.4±78.70	1939.8±70.82	2539.74±183.5
	Minimum	1423	1103.03±156.53	1217.8±132.56	1556.3±83.76	2069.76±234.44
	Maximum	1695	1723.36±261.11	1957.5±142.39	2331.7±168.5	3002.41±256.27
Width (95%)	Mean	1882	1359.10±86.52	1493.99±149.77	1956.30±107.48	2656.67±135.87
	Minimum	1672	1062.84±102.60	1148.71±285.92	1649.61±161.55	2121.82±302.14
	Maximum	2083	1699.89±149.02	1869.21±219.10	2331.79±233.75	3217.92±258.34
Depth (95%)	Mean	1728	1612.79±97.15	1790.34±92.60	2256.51±70.22	2746.34±94.79
	Minimum	1630	1251.87±87.40	1444.14±133.99	1909.18±111.07	2220.79±208.37
	Maximum	1950	1962.62±302.68	2162.50±224.99	2641.69±177.53	3213.27±194.21

like that of other virtual groups, was excessive compared to the experimental group.

The analysis of virtual motoneurons was extended to distribution emergent parameters (Fig. 5). Sholl-like plots of the number of bifurcations or terminations versus branch order or path distance yielded classical bellshaped curves for all real and virtual neurons. As an example, we report the dependence of the average number of branches (bifurcating and terminating) versus branching order (Fig. 5A). The experimental group had a peak of 66 branches at order 5, with a half-height width of 4.40. Hillman/PK neurons also had a peak at 5, with a value of 55.5 and a half-height width of 4.41. The Burke group peaked at order 4, with a value of 57.2 and a half-height width of 3.97. Finally, ArborVitae neurons had a peak value of 62.2 at order 6, and a half-height width of 4.95. Some of these characteristics reflect the effect of dendritic size (e.g., Burke neurons are slightly smaller than the real ones, thus the bellshaped distribution is narrower and peaks at a lower order; conversely, ArborVitae neurons are larger, and the distribution is wider and peaks at a higher order). Nonetheless, the good match of overall distribution shape as well as of peak position, value, and width between virtual neurons (particularly Hillman) and traced ones is non-trivial. The average branch diameter versus branch order distributions are reported in Fig. 5B. The traced cells showed a typical decay function that was well-matched by that observed for Burke and Hillman neurons. ArborVitae neurons displayed a similar decay at low branch orders, but reached a plateau at branch orders greater than 4.

Distributions of several parameters versus the path distance from the soma were also analyzed. As an example, the branch length sum, also yielding a bell-shaped distribution, is shown (Fig. 5C). The experimental group peaked at 900  $\mu$ m with a value of 22,640  $\mu$ m, and a half-height width of 912  $\mu$ m. The Hillman group had an identical peak position and half-height width, but a lower peak value (19,048  $\mu$ m). Burke neurons had a lower peak value (14,130  $\mu$ m) and position (700  $\mu$ m) relative to the experimental group, but a near-identical

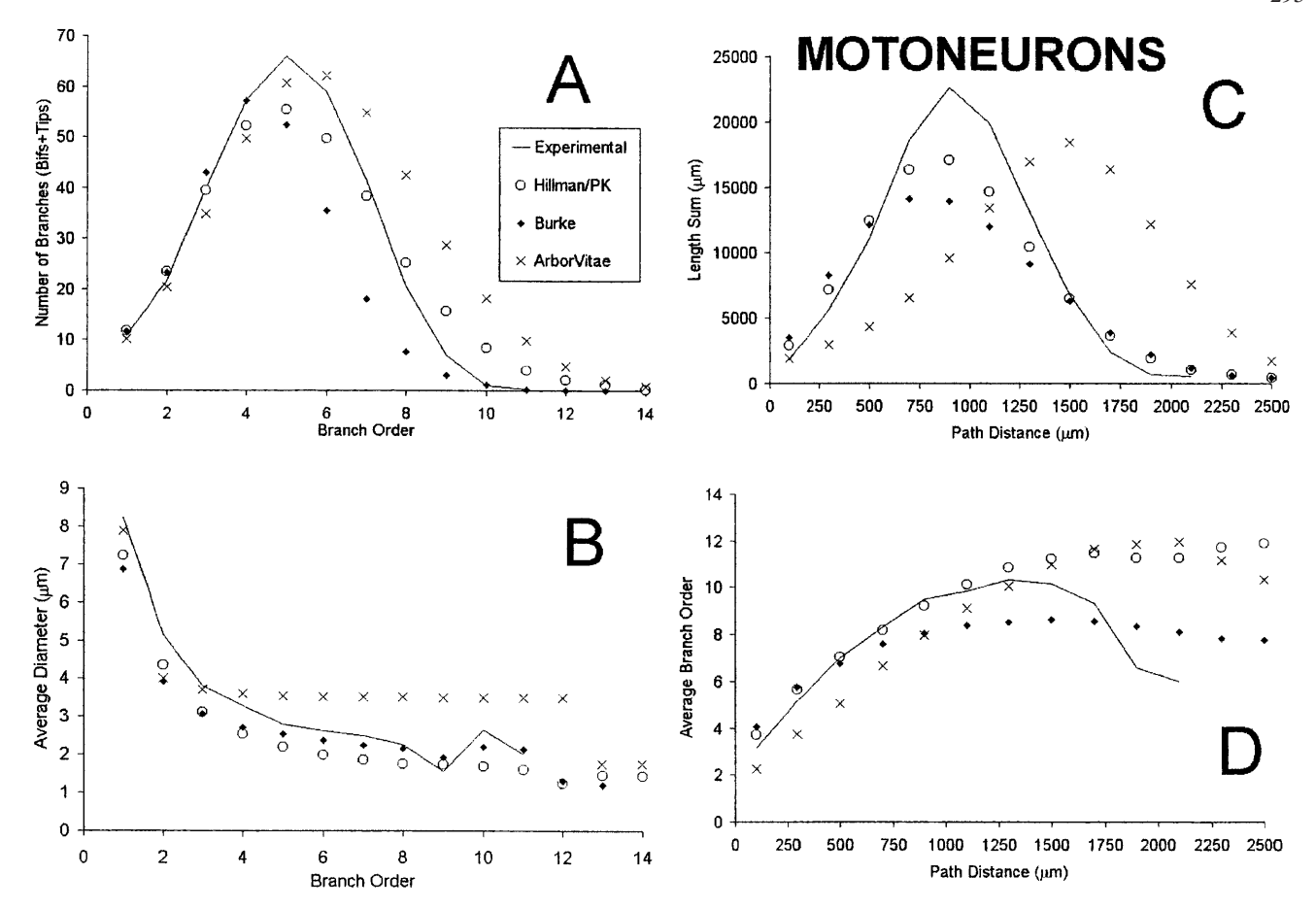


**Fig. 5A–D** Distribution emergent parameters for motoneurons (empty circles Hillman/PK; full diamonds: Burke; crosses Arbor-Vitae; line real neurons). **A** Number of branches versus branch order. **B** Branch diameter versus branch order. **C** Average sum of dendritic length versus path distance from the soma a. **D** Branch order versus path distance

half-height width (916 µm). Finally, as for the Sholl scatterplot, ArborVitae motoneurons had their center shifted farther from the soma (1500 µm), and a wider distribution (1,210 µm), although the peak value (18,442 µm) was the closest to the experimental measurement. Finally, the average branch order versus the path distance was examined (Fig. 5D). In real motoneurons the branch order increased almost linearly with the path distance (initial slope: 0.0096 µm<sup>-1</sup>) and then started to plateau at about 1000 µm from the soma (at an approximate value of 10), eventually decreasing at  $>1,500 \mu m$ . All virtual groups faithfully reproduced the initial linear behavior (initial slopes of 0.0083, 0.0068, and 0.0070 μm<sup>-1</sup> for Hillman/PK, Burke, and ArborVitae, respectively) and the subsequent plateau (respectively with values of 11.2, 8.5, and 11.1 for the three algorithms). However, only Burke motoneurons also displayed a slight decrease at greater distances. Overall, the virtual motoneurons trends appeared more linear than those of real motoneurons.

Analysis of Purkinje cell emergent parameters

The statistical analysis of the scalar emergent parameters of Purkinje cells was performed in a analogous manner to that described for motoneurons. The larger variability of simulated data with respected to experimental data seemed to impact Purkinie cells more than motoneurons. In particular, several virtual neurons terminated with an excessively small number of bifurcations (~10, compared to an experimental average of >400), and overall small trees (data not shown). On the contrary, in fewer circumstances, virtual Purkinje cells grew out of proportion (several thousands of bifurcations). Since these instances are not observed in Nature, we generated a larger population of virtual neurons, and then excluded the hypotrophic (<20 bifurcations/cell) or hypertrophic cells (>8000 bifurcations/cell) from the analysis. The percentages of excluded neurons were 52% for the Hillman algorithm (all hypotrophic), 19% for the corrected Hillman algorithm (17% hypotrophic and 2% hypertrophic), 6% for the Burke algorithm (all hypotrophic) and 10% for the ArborVitae algorithm (3.33% hypotrophic and 6.67% hypertrophic). Using the same criteria, none of the virtual motoneurons are excluded from the analysis. The uncorrected Hillman algorithm generated virtual neurons that were an order of magnitude smaller than real Purkinje cells as measured by several parameters (Table 4). As with motoneurons, the introduction of the correction factor PK dramatically improved the quality of vir-

**Table 4** Scalar emergent parameters for Purkinje cells. Three real neurons and 9–12 groups of three Purkinje cells for each algorithms were analyzed. See Table 3 for explanation of terms

Parameter	Value	Exp. ( <i>n</i> =1×3)	Hillman (n=10×3) μ±σ	Hillman/Poliko (n=12×3) μ±σ	Burke ( $n=10\times3$ ) $\mu\pm\sigma$	ArborVitae ( $n=9\times3$ ) $\mu\pm\sigma$
Total length (µm)	Mean	9134.6	669.03±107.87	9089.6±7984.36	9658.8±5862.2	3247.08±315.07
	Minimum	8128.2	529.99±124.18	2132.3±1541.23	3064.5±1454.4	1623.84±775.18
	Maximum	10,880.6	848.28±134.03	16,310±15,860	20,457±14,907	4607.32±811.78
Total area (μm²)	Mean	42,278	2999.19±498.31	35,578±31,140	42,882±25,788	11321.8±986.01
	Minimum	34,167	2431.35±613.47	8495.0±6113.91	13,472±6435	6011.5±2721.8
	Maximum	50,588	3735.72±613.14	63,591±62,532	90,715±65,594	15,870±2606
Asymmetry	Mean	0.50	0.46±0.05	0.51±0.02	0.54±0.01	0.54±0.01
	Minimum	0.49	0.41±0.07	0.49±0.02	0.51±0.02	0.53±0.02
	Maximum	0.51	0.50±0.05	0.54±0.02	0.57±0.02	0.56±0.02
No. of Bifurcations	Mean	436	32.6±5.76	442.19±389.26	446.27±269.81	367.52±33.81
	Minimum	417	25.9±5.24	102.75±72.06	142.6±69.97	180.22±84.87
	Maximum	472	41.6±7.42	796.08±776.69	945.2±684.12	518.78±85.85
Maximum order	Mean	27	9.7±0.83	23.81±5.12	23.37±4.10	43.78±5.21
	Minimum	25	8.7±1.1	17.17±3.98	18.5±3.38	34.56±11.50
	Maximum	30	10.9±0.83	29.58±7.26	28.6±8.06	50.78±5.86
Average path to tips (µm)	Mean	208.77	75.17±4.8	138.76±23.14	145.01±20.11	85.43±5.44
	Minimum	187.34	67.24±6.6	106.97±18.72	121.5±22.31	70.24±13.70
	Maximum	231.44	84.01±7.3	164.69±29.93	170.76±23.85	97.97±6.95
Average distane to tips (µm)	Mean	149.11	50.09±3.18	72.08±6.98	82.49±8.91	50.41±2.54
	Minimum	139.31	41.73±4.44	59.91±7.02	72.54±10.40	39.1±8.82
	Maximum	161.66	58.18±6.17	83.88±9.38	93.28±11.30	59.95±5.59
Maximum distance to tips ( $\mu m$ )	Mean	277.56	84.42±8.18	158.83±29.27	194.97±28.41	95.21±5.49
	Minimum	252.85	70.90±8.54	120.22±20.12	154.38±28.64	74.53±18.50
	Maximum	307.94	99.08±13.0	198.85±45.83	234.64±36.17	112.4±7.95
Height (95%)	Mean	218.50	80.67±7.33	142.72±27.69	168.82±35.73	77.19±9.45
	Minimum	210.50	63.77±9.55	108.30±31	120.59±39.69	54.59±11.10
	Maximum	229.50	100.60±12.6	180.08±43.95	222.41±53.34	103.9±15.30
Width (95%)	Mean	222.33	72.56±11.0	136.45±21.9	170.19±18.53	68.7±4.52
	Minimum	207.50	60.16±7.71	92.63±18.37	147.42±25.44	52.45±9.81
	Maximum	240.00	87.63±18.7	176.45±33.85	192.3±23.43	86.09±12.30
Depth (95%)	Mean	20.17	34.73±7.1	86.56±25.79	117.48±33.31	0±0
	Minimum	17.50	23.94±5.5	55.55±18.47	88.79±26.62	0±0
	Maximum	23.50	44.39±10.7	114.98±40.74	152.93±48.71	0±0

tual Purkinje cells. The mean of all the scalar parameters of the Hillman/PK Purkinje cells that did not depend on angles, with the exception of the path to tips, had an average value close to the experimental measurement, and in most case largely within 0.5 standard deviations. However, in many cases the standard deviation had a value comparable to that of the average itself, implying large variability in the data. In addition, none of the scalar measurements involving Euclidean distance in the real cells was accurately reproduced by the Hillman/PK algorithm (Table 4).

The analysis of Purkinje cells generated with Burke's algorithm yielded similar results to those for the corrected Hillman algorithm (Table 4). The average values of mean length, surface area, and number of bifurcations nicely reproduced the traced data, while the average distance and path to tips and the Euclidean sizes were over a standard deviation shorter than the experimental data. Purkinje cells generated with ArborVitae were very small compared to the real cells, an opposite trend from that observed for motoneurons. The total length, area, number of bifurcations, height and width, all had values

significantly smaller than the corresponding measurements in the real neurons (in ArborVitae the depth of Purkinje cells was imposed to zero by a global constraint of planarity). However, both the mean and extreme values of branch order were larger for ArborVitae neurons than for real Purkinje cells. Interestingly, the variability of ArborVitae Purkinje cells, although larger than in the original data, is significantly smaller than that of groups generated with L-Neuron algorithms (Table 4).

Distribution emergent parameters of Purkinje cells were analyzed as for motoneurons (Fig. 6). Sholl-like plots of the summed number of bifurcations and terminations versus branch order yielded bell-shaped distributions for real and L-Neuron cells (Fig. 6A). Real neurons data displayed an irregular peak front, with maxima at 15 and at 18 (average peak value of 64), and a half-height width of 13.5. Hillman/PK cells reproduced well the peak position (14), but the distribution was flattened (peak of 49.8, half-height width of 16.2). In contrast, Burke cells had a lower peak position (12), but better peak value (68.5) and half-height width (12.1). ArborVitae neurons had also bell-shaped distributions, but with an

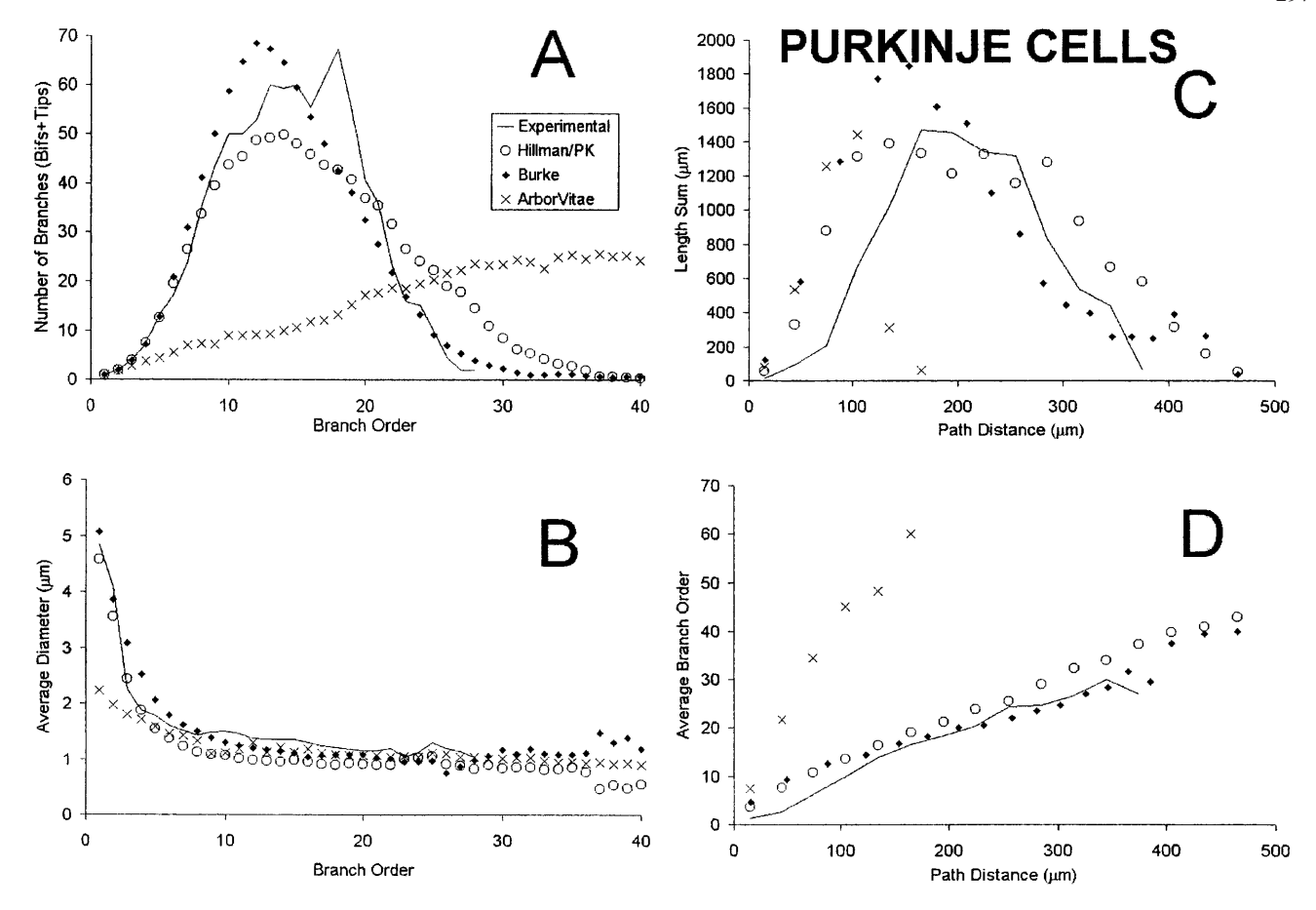


**Fig. 6A–D** Purkinje cell distribution emergent parameters (symbols as in Fig. 5). **A** Number of branches versus branch order. **B** Branch diameter versus branch order. **C** Average sum of dendritic length versus path distance from the soma. **D** Branch order versus path distance

exceedingly high value for peak position and width. The dependency of average branch diameters on branch order followed a classical decay trend for all cell groups (Fig. 6B). For this distribution, the Hillman and Burke algorithms yielded the best simulation of diameter values near the soma; Hillman and ArborVitae produced best values between order 4 and 8; and ArborVitae and Burke reproduced most accurately the plateau behavior at the highest order values.

The analysis of emergent parameter versus path distance followed similar trends. The bell-shaped distribution plots of dendritic length sum (Fig. 6C) had experimental values of 165 μm for peak position, 1,472 μm for peak height, and 184.5 μm for peak width. Hillman Purkinje cells displayed accurate values of peak position (135 μm) and height (1390 μm), but an excessive width (270 μm). Burke neurons had accurate peak position (155 μm) and width (176.5 μm), but excessive peak height (1848 μm). ArborVitae distribution data yielded correct values of peak height (1441 μm), but smaller than normal values for peak position (105 μm) and width (72 μm). Finally, the distribution of average branch order versus path distance (Fig. 6D) displayed regular linear

trends for all groups of neurons. The slope of the traced data (0.081  $\mu m^{-1}$ , R<sup>2</sup>=0.96) was well matched with that of the L-Neuron algorithms (Hillman: 0.087  $\mu m^{-1}$ , R<sup>2</sup>=0.99; Burke: 0.074  $\mu m^{-1}$ , R<sup>2</sup>=0.97), but not with Arbor-Vitae (0.336  $\mu m^{-1}$ , R<sup>2</sup>=0.97).

The highly planar structure of the Purkinje dendritic trees, which is not captured by local constraints, may contribute to some of the discrepancies between real and virtual neurons observed in the case of Purkinje cells (e.g. last five parameters in Table 4). Thus, we compared traced cells as well as Hillman virtual cells with groups of neurons generated with modifications of Hillman's algorithm that affected angles. In the Tamori modification, bifurcation amplitude angles are not measured empirically, but calculated based on Rall's power coefficient (Tamori 1993). Additional modifications were investigated by the analysis of different tropism influences. First, depth tropism (with a weight of 0.1 relative to the endogenous growth direction) was added to push dendrites towards the plane of the soma and first stem. Next, a second tropism influence (with a weight of 0.01) was imposed to push dendrites away from the soma. Sets of Purkinje cells grouped by three were generated with these modified algorithms and statistically analyzed. As expected, the emergent parameters not dependent on angles were unaffected by the algorithm modifications (not shown). The angle-dependent scalar emergent parameters for the experimental, original Hillman/PK-generated, and modified Hillman/PK Purkinje cells are summa-

**Table 5** Variations of the Hillman algorithm: angle-dependent scalar emergent parameters for Purkinje cells. The first two columns are data from experimental neurons and Hillman/PK neurons. The third column represents neurons generated with the Ta-

mori modification of the Hillman/PK algorithm. Data in the fourth column involves the addition of depth tropism to the Tamori algorithm. In the last data column, a second form of tropism (somatocentric) was added to the Tamori plus depth tropism algorithm

Parameter	Value	Exp. ( <i>n</i> =1×3)	Hillman/Poliko (n=12×3) μ±σ	Hillman/Tamori (n=12×3) μ±σ	Depth Tropism (n=13×3) μ±σ	Soma Tropism ( <i>n</i> =13×3) μ±σ
Average distance to tips (µm)	Mean	149.11	72.08±6.98	101.09±17.86	103.73±16.23	116.89±12.21
	Minimum	139.31	59.91±7.02	79.762±19.49	58.12±11.10	81.434±13.54
	Maximum	161.66	83.88±9.38	123.42±25.66	180.53±25.23	161.62±18.77
Maximum distance to tips (μm)	Mean	277.56	158.83±29.27	187.32±41.09	196.78±42.72	223.03±37.60
	Minimum	252.85	120.22±20.12	128.01±40.34	95.74±36.98	147.49±39.87
	Maximum	307.94	198.85±45.83	249.88±65.28	352.56±65.03	350.76±49.10
Height (95%)	Mean	218.50	142.72±27.69	166.66±36.35	195.92±51.03	202.99±49.44
	Minimum	210.50	108.30±31	116.78±36.36	61.19±30.55	95.33±32.12
	Maximum	229.50	180.08±43.95	222.60±60.57	337.56±64.86	340.87±54.68
Width (95%)	Mean	222.33	136.45±21.9	133.40±39.29	158.12±33.90	170.25±46.77
	Minimum	207.50	92.63±18.37	94.71±33.93	69.71±29.74	88.36±29.98
	Maximum	240.00	176.45±33.85	169.40±46.18	360.67±68.07	356.18±53.05
Depth (95%)	Mean	20.17	86.56±25.79	80.31±27.96	6.64±2.51	16.72±5.90
	Minimum	17.50	55.55±18.47	40.38±32.23	1.57±0.68	7.02±2.36
	Maximum	23.50	114.98±40.74	127.30±53.32	18.40±3.35	46.96±8.72

rized in Table 5. The Tamori modification of Hillman's algorithm improved the simulation of experimental structures as assessed by all parameters (mean and range), with the exception of dendritic width, which remained unaltered. The addition of depth tropism to the Tamori-modified Hillman algorithm only affected tree size, by reducing the depth (as expected) and consequently enlarging height and width ("ironing" effect). These changes further improved the modeling of experimental data. Finally, because depth tropism pushed dendrites, on average, towards the soma, the additional soma tropism correction aimed at compensating this effect. All emergent parameters (last column of Table 5) demonstrated a further enhancement of the resulting virtual morphologies. Thus, the best fit to experimental data was achieved by adding the Tamori and tropism modifications to the Hillman algorithm.

The above algorithm modifications improved the scalar Euclidean measurements of dendritic structure, without affecting angle-independent parameters. Thus, we used distributions emergent parameters based on Euclidean distance (as opposed to path) to investigate other potential effects of these algorithm variations (Fig. 7). Since most distribution parameters based on Euclidean distance had similar trends, we report here only two examples. The dependence of the average sum of surface area within a distance bin (spherical shell) on the distance itself resulted in an irregular bell-shaped distribution for all algorithms (Fig. 7A). The experimental group had a peak at 130  $\mu$ m (with a value of 5,042  $\mu$ m<sup>2</sup>) and a half-height peak width of 173 µm. The unmodified Hillman/PK Purkinje cells and the Tamori modification yielded almost identical results with a good match of the traced data (peak position, value, and width of 110 µm, 5,402 µm<sup>2</sup>, and 168 µm, respectively). Unexpectedly, depth tropism decreased the accuracy of the simulation

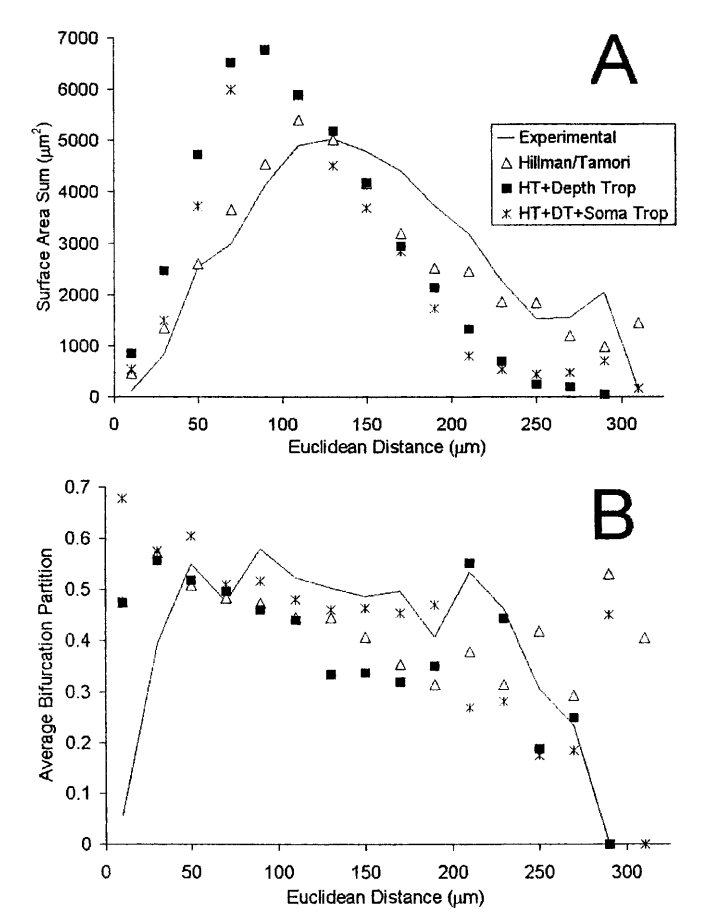


**Fig. 7A, B** Angle-dependent distribution emergent parameters for Purkinje cells (*empty triangles* Tamori modification, *full squares* addition of depth tropism, *asterisks* further addition of somatocentric tropism, *line* real neurons). The unmodified Hillman/PK algorithm produced results overlapping with those from the Tamori modification. **A** Average surface area versus Euclidean distance. **B** Average bifurcation partition versus Euclidean distance

(peak position, value, and width of 90 μm, 6,763 μm<sup>2</sup>, and 125 µm, respectively). The further addition of somatocentric tropism did not correct this effect (peak position, value, and width of 90 µm, 6,781 µm<sup>2</sup>, and 111 μm, respectively). The analysis of the average bifurcation partition versus Euclidean distance yielded qualitatively similar results (Fig. 7B). The distribution for the real neurons had a skewed square shape with a rapid rise, a slow decay, and a rapid fall. The virtual neuron data reproduced this trend, without any relevant difference due to the influence of algorithm modifications. The noise in the data is due to the usual higher variability observed in simulated dendrites. Thus, although the Tamori variation and the addition of tropism improve several angle-dependent morphological properties of virtual neurons, they have little or negative effect on more subtle aspects of dendritic geometry.

### **Discussion**

This paper describes the first extensive morphological analysis that compares complete, algorithmically generated neurons with a limited set of experimentally traced neurons. To the extent that the algorithms actually succeed in statistically simulating the original anatomical structures, the computer generation of virtual neurons achieves two important goals. First, it provides a great deal of data compression, because a set of basic parameters employed by the algorithms describes an entire morphological class more compactly than the description of a single traced neuron in standard digitized format (Ascoli 1999; Ascoli and Krichmar 2000). Second, it naturally amplifies the data, since an arbitrarily large number of virtual neurons can be generated from a finite data set (Senft and Ascoli 1999; Ascoli 1999). These features may have great impact on the development of neuromorphological databases (Ascoli et al. 2001).

The exercise in data extraction to measure basic parameter distributions from digital files demonstrated that the neuroanatomical descriptions on which L-Neuron and ArborVitae are based are consistently and completely defined. Thus, two morphological classes as different as motoneurons and Purkinje cells could be represented in each algorithm with different statistical distributions of the same set of parameters. The extraction of basic parameters also indicated the usefulness of the mixture of distributions allowed for by L-Neuron. In contrast, the extensive use of truncated Gaussian functions to fit skewed distributions was neither efficient nor accurate. The implementation of more refined statistical functions, such as gamma distributions, may constitute an important future addition to all algorithms. As an important side result, we extended Burke's analytical approach, originally designed for motoneurons, to Purkinje cells. All Burke parameters could be described and fitted with simple statistical distributions for Purkinje cells as well as for motoneurons, thus suggesting that Burke's algorithm (and likewise Hillman's and ArborVitae) reflect anatomical rules and mechanisms that apply to different morphological classes.

For both motoneurons and Purkinje cells, the simple description proposed by Hillman (1979) failed to generate neurons of adequate size and structure. However, a single correction factor in Rall's power law dramatically improved the algorithm. The modified Hillman algorithm generated motoneurons and Purkinje cells with accurate emergent values of dendritic length, asymmetry, and number of bifurcations. Hillman-generated motoneurons also displayed correct values for maximum order and average terminal path and distance from the soma. In addition, Hillman motoneurons and Purkinje cells displayed distribution emergent parameters that behaved in qualitatively (and in most cases, quantitatively) similar manners as the corresponding real neurons with respect to both branch order and path distance. With minor modifications to Hillman's algorithm (e.g., Tamori's variation and tropism influence), the fitting of angle-dependent scalar parameters to the experimental data also improved significantly. Taken as a whole, these observations indicate that the modified Hillman algorithms accurately capture a remarkable amount of morphological properties of both motoneurons and Purkinje cells.

The Burke algorithm yielded results comparable to the corrected Hillman algorithm, as expected from the similarities between the algorithms, especially in their crucial local dependence on branch diameters. However, a few differences were also noted. For both motoneurons and Purkinje cells, Burke's algorithm was superior to Hillman's in describing dendritic area, but inferior in describing tree asymmetry. For other emergent parameters a clear pattern did not emerge across cell classes, possibly suggesting more subtle influences on specific morphological aspects and warranting further investigations. It is likely that the addition of tropism to the Burke algorithm would improve the quality of generated Purkinje cells in an analogous fashion to that observed for the Hillman algorithm. A complete understanding of the strength and weakness of each algorithm could lead to the design of a hybrid, best performing L-Neuron algorithm. ArborVitae also showed potential in describing dendritic morphology. It would be tempting to speculate on the relative qualities and biases of the L-Neuron predominantly local / single-cell approach and the ArborVitae mainly global/population-based approach. However, the contrasting indications provided by the two different cell classes in this case prevent firm conclusions. For example, ArborVitae motoneurons had larger values for length, surface area, and number of bifurcations than both L-Neuron and real motoneurons; however, Arbor-Vitae Purkinie cells had smaller values in all size-related parameters (but higher maximum order) than both L-Neuron and real Purkinje cells. One possible explanation is that ArborVitae basic parameters are more difficult to measure precisely from the original data because of their global definitions, as discussed in previous sections. On the other hand, once the basic parameters are fine-tuned, the ArborVitae generation of neuronal populations can lead to the simulation of spatial assembly and network formation (Fig. 4E and Senft and Ascoli 1999).

Although a great deal of morphological complexity was encapsulated in L-Neuron and ArborVitae, it is important to discuss the neuroanatomical features that these algorithms have thus far failed to reproduce. The most important aspect is the excessive variability of the simulated data. To a certain extent, the greater data variability observed in the modeled structures as compared to the real neurons is a consequence of the enacted data amplification (for one group of three or six real neurons, 10 or more groups of virtual neurons were generated). Still, the observed morphological variability in virtual neurons is much too great. For example, the difference in number of bifurcations between the largest and the smallest of the six real motoneurons was 59, and the same number for the three real Purkinje cells was 55. On average, this difference for an equivalent group of (six or three) virtual neurons was 612 for motoneurons and 123 for Purkinje cells (see Tables 3, 4). Natural neurons might have a more limited variability because they obey both local and global constraints whereas the algorithms we tested mainly focus on one class of constraints. If this is the case, a future implementation of a hybrid L-Neuron/ArborVitae algorithm could provide a solution to this discrepancy. Interestingly, the morphological variability is larger in virtual Purkinje cells than in virtual motoneurons. This may be due to the fact that rat Purkinje cells have a single dendritic tree, while motoneurons have on average more than ten. Thus, simulated Purkinje cells are particularly susceptible, within the first few bifurcations, to the stochastic sampling of data. An unfortunate set of sampled values can cause, in Purkinje cells, the sudden termination of an entire neuron, whereas in motoneurons it would only cause the termination of one in many trees. The simulation logs confirmed this inference. Due to the small number of available experimental data of completely traced Purkinje cells, it is hard to hypothesize the real extent of their size range. However, in a living tissue, a Purkinje cell that randomly stopped growing at a very early stage of maturation would be likely pruned back and reabsorbed to recycle the metabolic material (and therefore never be traced). Hence, our decision to conform to the available data, thus excluding from the analysis all virtual neurons smaller than 5% (or greater than 2,000%) of the experimental average.

Other specific aspects of dendritic morphology showed significant discrepancies between real and generated neurons. For example, in Purkinje cells, but not in motoneurons, L-Neuron algorithms consistently produced neurons with a maximum order that was lower than that of real cells by approximately 3.5 units (23.8 in Hillman and 23.4 in Burke as opposed to 27.0 in real Purkinje cells, see Table 4). However, the number of bifurcations did not follow this trend. In fact, when the relevant basic parameters (PK and Rall's power in Hillman,  $P_{ov}$  and  $P_{nov}$  in Burke) were artifactually changed to obtain an accurate correspondence of the maximum order between virtual and real neurons, the resulting number of

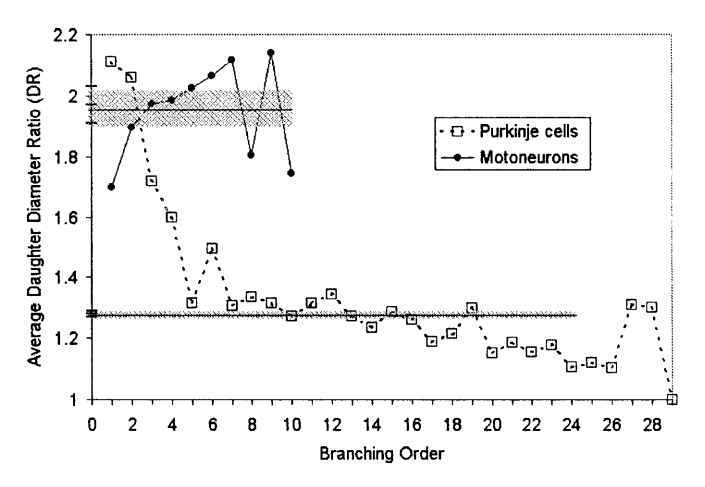


**Fig. 8** Distribution of daughter diameter ratio (DR) versus branch order (*full circles, continuous line* motoneurons, *empty square*, *broken line* Purkinje cells). Horizontal lines and gray areas represent the mean DR value (plus/minus standard error) measured across all orders

bifurcation of virtual neurons almost tripled (data not shown). These observations led us to hypothesize a nontrivial difference between real motoneurons and Purkinje cells. It is known that the relationship between total number of bifurcations and maximum branching order in a tree is linked to the tree asymmetry (van Pelt et al. 1992). Locally, tree asymmetry is reflected in the bifurcation partition, which is in turn directly bound to the daughter diameter ratio (basic parameter DR): a higher value of DR corresponds to a higher partition, and thus a higher maximum branching order given a fixed number of bifurcations. Thus, we hypothesized that in Purkinje cells, but not in motoneurons, the daughter diameter ratio in the first four orders of branching is significantly higher than in the rest of the tree. Such a characteristic would not be captured by the average distributions used in L-Neuron, and would cause a higher number of bifurcations and/or lower maximum branch order in virtual neurons. This hypothesis was directly tested by analyzing the experimental dependence of DR on branch order in both Purkinje cells and motoneurons (Fig. 8).

The experimental data confirmed this hypothesis: the daughter diameter ratio in Purkinje cells starts at values over 2 at orders 1–2, and then drops rapidly, reaching a steady level of ~1.28 after order 4. Because the grand average is weighted by the number of bifurcations, and such a number is largest at orders 10–20 (Fig. 6A), the initial values of DR is completely invisible in the overall DR distribution (gray area in Figure 8). In contrast, in motoneurons, the dependency of DR on the order has the opposite trend. In addition, the larger number of dendritic trees stemming out of the soma provides DR values at lower branching order with a more significant weight. As a result, the overall distribution of DR reflects the local values in all regions of the dendritic tree more accurately. This observation explains several other measured discrepancies between some groups of virtual Purkinje cells and the real neurons, such as in the average path and distance to tips. The same trends are not observed in ArborVitae, where the dependency on both local constraints and branch diameter is almost entirely lacking. The peculiar distribution of DR versus branching order in the experimental data corresponds to the structure of a main, thick dendrite and several smaller branches; this feature is only present in the first 3–4 branching orders of Purkinje cells (Rapp et al. 1994), and not at all in motoneurons. This rationalization is an example of the usefulness of model-driven research strategies. From the point of view of algorithmic design, it suggests that the Hillman algorithm can be improved by inserting a dependency of DR on branching order.

A final source of discrepancies between real and virtual Purkinje cells consists of the reduced Euclidean size of virtual trees compared to real ones, even after the improvements by the Tamori variation and the tropism influence. One interesting possibility is that this residual discrepancy may be due to a space-filling phenomenon. In nature, no two dendritic branches can occupy the same physical position. In addition, during growth, real neurons may actively seek to avoid growing too close to each others by chemical mechanisms of mutual detection and contact inhibition (Sestan et al. 1999). This could be important to pack dense networks in a limited tissue, but might also influence single dendritic trees, pushing them to occupy wider space. In the generation of virtual neurons, these space-packing issues are not currently addressed. The future addition of this type of constraint is also expected to improve the results.

Acknowledgements This work was supported in part by Human Brain Project grant R01-NS39600, funded jointly by NINDS and NIMH (National Institutes of Health). We are thankful to Drs. Robert E. Burke and Moshe Rapp for making the real morphological data of motoneurons and Purkinje cells, respectively, available to us. GAA acknowledges the hospitality of the Scuola Normale Superiore of Pisa (Italy), where part of the data analysis was performed.

# **References**

- Ascoli GA (1999) Progress and perspective in computational neuroanatomy. Anat Rec 257:195–207
- Ascoli GA (ed) (2001) Computational neuroanatomy: principles and methods. Humana Press, Totowa, NT (in press)
- Ascoli GA, Krichmar JL (2000) L-Neuron, a modeling tool for the efficient generation and parsimonious description of dendritic morphology. Neurocomputing, 32/33:1003–1011
- Ascoli GA, Krichmar JL, Nasuto SJ, Senft SL (2001) Generation, description, and storage of dendritic morphology data. Phil Trans R Soc B Biol Sci 356(1412):1131–1145
- Bower JM, Beeman D (1998) The Book of GENESIS: exploring realistic neural models with the General Simulation System. Springer, Berlin Heidelberg New York
- Burke RE, Marks WB, Ulfhake B (1992) A parsimonious description of motoneurons dendritic morphology using computer simulation. J Neurosci 12:2403–2416

- Cullheim S, Fleshman JW, Glenn LL, Burke RE (1987) Membrane area and dendritic structure in type-identified Triceps Surae alpha motoneurons. J Comp Neurol 255:68–81
- Hillman DE (1979) Neuronal shape parameters and substructures as a basis of neuronal form. In: Schmitt F (ed) The Neurosciences, 4th Study Program, MIT Press, Cambridge, Mass., pp 477–498
- Hillman DE (1988) Parameters of dendritic shape and substructure: intrinsic and extrinsic determination? In: Lasek RJ, Black MM (eds) Intrinsic determinants of neuronal form and function. Liss, New York pp 83–113
- Koch C, Segev I (eds) (1998) Methods in neural modeling: from ions to networks, 2nd edn. MIT Press Cambridge, Mass
- Mainen ZF, Sejnowski T (1996). Influence of dendritic structure on firing pattern in model neocortical neurons. Nature 382: 363–366
- Mel BW, Ruderman DL, Archie KA (1998) Translation-invariant orientation tuning in visual 'complex' cells could derive from intradendritic computations. J Neurosci 18:4325–4334
- Ooyen A van, Willshaw DJ, Ramakers GJA (2000) Influence of dendritic morphology on axonal competition. Neurocomputing, 32/33:255–260
- Pelt J van, Uylings HBM, Verwer RWH, Pentney RJ, Woldenberg MJ (1992) Tree asymmetry – A sensitive and practical measure for binary topological trees. Bull Math Biol 54:759– 784
- Pelt J van, Dityatev AE, Uyilings HBM (1997) Natural variability in the number of dendritic segments: model-based inferences about branching during neurite outgrowth. J Comp Neurol 387:325–340
- Peterson DA (1999) Quantitative histology using confocal microscopy: implementation of unbiased stereology procedures. Methods 18:493–507
- Rall W (1959) Branching dendritic trees and motoneurons membrane resistivity. Exptl Neurol 1:491–527
- Rapp M, Segev I, Yarom Y (1994) Physiology, morphology, and detailed passive models of guinea-pig cerebellar Purkinje cells. J Physiol 474:101–118
- Scorcioni R, Krichmar JL, Ascoli GA (2001) Algorithmic extraction of morphological statistics from electronic archives of neuroanatomy. Lecture Notes Computer Science. (in press)
- Senft SL (1997) A statistical framework for presenting developmental neuroanatomy. In: Donahoe J, Dorsel VP (eds) Neuralnetwork models of cognition: biobehavioral foundations Elsevier Press, Amsterdam New York, pp 37–57
- Senft SL, Ascoli GA (1999) Reconstruction of brain networks by algorithmic amplification of morphometry data. Lecture Notes Computer Science 1606:25–33
- Sestan N, Artavanis-Tsakonas S, Rakic P (1999) Contact-dependent inhibition of cortical neurite growth mediated by notch signalling. Science 286(5440):741–746
- Sholl DA (1953) Dendritic organization in the neurons of the visual and motor cortices of the cat. J Anat 87:387–406
- Stuart G, Spruston N, Sakmann B, Hausser M. (1997) Action potential initiation and back-propagation in neurons of the mammalian CNS. Trends Neurosci 20:125–131
- Tamori Y (1993) Theory of dendritic morphology. Physiol Rev E 48:3124–3129
- Uylings HBM, Ruiz-Marcos A, Pelt J van (1986) The metric analysis of three-dimensional dendritic tree patterns: a methodological review. J Neurosci Methods 18:127–151
- Winslow JL, Jou SF, Wang S, Wojtowicz JM (1999) Signals in stochastically generated neurons. J Comput Neurosci 6:5–26